

AN AUGMENTED LAGRANGIAN PRECONDITIONER FOR THE MAGNETOHYDRODYNAMICS EQUATIONS AT HIGH REYNOLDS AND COUPLING NUMBERS *

FABIAN LAAKMANN[†], PATRICK E. FARRELL[‡], AND LAWRENCE MITCHELL[§]

Abstract. The magnetohydrodynamics (MHD) equations are generally known to be difficult to solve numerically, due to their highly nonlinear structure and the strong coupling between the electromagnetic and hydrodynamic variables, especially for high Reynolds and coupling numbers. In this work, we present a scalable augmented Lagrangian preconditioner for a finite element discretization of the **B-E** formulation of the incompressible viscoresistive MHD equations. For stationary problems, our solver achieves robust performance with respect to the Reynolds and coupling numbers in two dimensions and good results in three dimensions. We extend our method to fully implicit methods for time-dependent problems which we solve robustly in both two and three dimensions. Our approach relies on specialized parameter-robust multigrid methods for the hydrodynamic and electromagnetic blocks. The scheme ensures exactly divergence-free approximations of both the velocity and the magnetic field up to solver tolerances. We confirm the robustness of our solver by numerical experiments in which we consider fluid and magnetic Reynolds numbers and coupling numbers up to 10,000 for stationary problems and up to 100,000 for transient problems in two and three dimensions.

Key words. Magnetohydrodynamics (MHD), multigrid, augmented Lagrangian

AMS subject classifications. 65N55, 65N30, 65F10, 65F08

1. Introduction. In this work, we consider the incompressible viscoresistive magnetohydrodynamics (MHD) equations on a simply-connected polytopal domain $\Omega \subset \mathbb{R}^d$, $d \in \{2, 3\}$. In the stationary three-dimensional setting, we investigate the formulation

$$\begin{aligned}
 (1.1a) \quad & -\frac{2}{\text{Re}} \operatorname{div} \varepsilon(\mathbf{u}) + \mathbf{u} \cdot \nabla \mathbf{u} + \nabla p + S \mathbf{B} \times (\mathbf{E} + \mathbf{u} \times \mathbf{B}) = \mathbf{f}, \\
 (1.1b) \quad & \operatorname{div} \mathbf{u} = 0, \\
 (1.1c) \quad & \mathbf{E} + \mathbf{u} \times \mathbf{B} - \frac{1}{\text{Re}_m} \operatorname{curl} \mathbf{B} = \mathbf{0}, \\
 (1.1d) \quad & \operatorname{curl} \mathbf{E} = \mathbf{0}, \\
 (1.1e) \quad & \operatorname{div} \mathbf{B} = 0.
 \end{aligned}$$

Here, $\mathbf{u} : \Omega \rightarrow \mathbb{R}^3$ denotes the velocity, $p : \Omega \rightarrow \mathbb{R}$ the fluid pressure, $\mathbf{B} : \Omega \rightarrow \mathbb{R}^3$ the magnetic field, $\mathbf{E} : \Omega \rightarrow \mathbb{R}^3$ the electric field, Re the fluid Reynolds number, Re_m the magnetic Reynolds number, S the coupling number, $\mathbf{f} : \Omega \rightarrow \mathbb{R}^3$ a source term and $\varepsilon(\mathbf{u}) = \frac{1}{2}(\nabla \mathbf{u} + \nabla \mathbf{u}^\top)$. The system is completed with the boundary conditions

$$(1.2) \quad \mathbf{u} = \mathbf{0}, \quad \mathbf{E} \times \mathbf{n} = \mathbf{0}, \quad \mathbf{B} \cdot \mathbf{n} = 0 \quad \text{on } \partial\Omega,$$

where \mathbf{n} is the unit outer normal vector. The above formulation based on the electric and magnetic fields was first rigorously analyzed by Hu et al. [29]. It is straightforward

*Submitted to the editors May 3, 2021.

Funding: The first author was supported by the EPSRC Centre for Doctoral Training in Partial Differential Equations: Analysis and Applications, grant EP/L015811/1. The second author was supported by EPSRC grants EP/V001493/1 and EP/R029423/1.

[†]Mathematical Institute, University of Oxford, Oxford, UK (fabian.laakmann@maths.ox.ac.uk).

[‡]Mathematical Institute, University of Oxford, Oxford, UK (patrick.farrell@maths.ox.ac.uk).

[§]Department of Computer Science, Durham University, Durham, UK (lawrence.mitchell@durham.ac.uk).

to derive the two-dimensional formulation from this work, which is given by

$$(1.3a) \quad -\frac{2}{\text{Re}} \operatorname{div} \varepsilon(\mathbf{u}) + \mathbf{u} \cdot \nabla \mathbf{u} + \nabla p + S \mathbf{B} \times (E + \mathbf{u} \times \mathbf{B}) = \mathbf{f},$$

$$(1.3b) \quad \operatorname{div} \mathbf{u} = 0,$$

$$(1.3c) \quad E + \mathbf{u} \times \mathbf{B} - \frac{1}{\text{Re}_m} \operatorname{curl} \mathbf{B} = 0,$$

$$(1.3d) \quad \operatorname{curl} E = \mathbf{0},$$

$$(1.3e) \quad \operatorname{div} \mathbf{B} = 0,$$

subject to the boundary conditions

$$(1.4) \quad \mathbf{u} = \mathbf{0}, \quad E = 0, \quad \mathbf{B} \cdot \mathbf{n} = 0 \quad \text{on } \partial\Omega.$$

Note that E is a scalar field in 2D and there exist two different curl operators given by

$$(1.5) \quad \operatorname{curl} \mathbf{B} = \partial_x B_2 - \partial_y B_1, \quad \operatorname{curl} \varphi = \begin{pmatrix} \partial_y \varphi \\ -\partial_x \varphi \end{pmatrix}$$

that correspond to the cross-products

$$(1.6) \quad \mathbf{A} \times \mathbf{B} = A_1 B_2 - A_2 B_1, \quad \mathbf{B} \times \varphi = \begin{pmatrix} B_2 \varphi \\ -B_1 \varphi \end{pmatrix}.$$

Other formulations include the current density $j = \mathbf{E} + \mathbf{u} \times \mathbf{B}$ [30] as an unknown or eliminate the electric field using equation (1.1c). In addition to the stationary case, we also consider the time-dependent version of (1.1) where the time-derivatives $\frac{\partial \mathbf{u}}{\partial t}$ and $\frac{\partial \mathbf{B}}{\partial t}$ are added to (1.1a) and (1.1d) respectively with suitable initial conditions $\mathbf{u}(\mathbf{x}, 0) = \mathbf{u}_0(\mathbf{x})$ and $\mathbf{B}(\mathbf{x}, 0) = \mathbf{B}_0(\mathbf{x}) \forall \mathbf{x} \in \Omega$. Note that it is a common assumption in MHD to neglect displacement currents $\frac{\partial \mathbf{E}}{\partial t}$ [25, Sec. 1.5].

The main contribution of this work is to provide block preconditioners for the models (1.1) and (1.3) with good convergence even at high Reynolds and coupling numbers. The performance relies on the following three (novel) approaches:

- 1.) We consider a fluid-Reynolds-robust augmented Lagrangian preconditioner for an $\mathbf{H}(\operatorname{div}) \times L^2$ -discretization of the Navier-Stokes equations that relies on a specialized multigrid method.
- 2.) We introduce a new monolithic multigrid method for the electromagnetic block.
- 3.) We discover that using the outer Schur complement which eliminates the (\mathbf{u}, p) block instead of the (\mathbf{E}, \mathbf{B}) block has crucial advantages for ensuring robustness for high parameters.

Furthermore, we show that our preconditioners extend in a straightforward manner to the time-dependent version of (1.1). This has the substantial advantage that the choice of the time-stepping scheme is no longer restricted by the ability to solve the linear systems. In particular, it allows the use of fully implicit methods for high Reynolds numbers and coupling parameters.

An important point for discretizations is the enforcement of the magnetic Gauss' law $\operatorname{div} \mathbf{B} = 0$ in the weak formulation, achieved in most cases by a non-physical Lagrange multiplier r [44]. However, in general a Lagrange multiplier only enforces the divergence constraint in a weak sense, which can cause severe problems for the discretization and numerical simulations [11, 17]. For the \mathbf{B} - \mathbf{E} formulation (1.1) Hu

et al. [29] show that both a Lagrange multiplier and an augmented Lagrangian term lead to a point-wise preservation of Gauss' law. In this work, we consider the latter approach by replacing (1.1d) with

$$(1.7) \quad \frac{1}{\text{Re}_m} \nabla \cdot \mathbf{B} + \mathbf{curl} \mathbf{E} = \mathbf{0}.$$

The literature proposes numerous numerical schemes and preconditioning strategies for the numerical solution of the different formulations. The most common approach is based on block preconditioners in both the stationary [32, 37, 38, 49, 48] and time-dependent [14, 16, 39] cases. Here, the main challenges are to find suitable approximations of one or more Schur complements and robust linear solvers for the inner auxiliary problems. Phillips et al. [39] simplify the Schur complement by the use of vector identities and approximate the remaining parts based on a spectral analysis. They report iteration counts for a stationary three-dimensional lid-driven cavity problem up to $\text{Re} = \text{Re}_m = 100$. A similar approach is used by Wathen and Greif in [48] where they construct an approximate inverse block preconditioner by sparsifying a derived formula for the exact inverse and drop low order terms. Here, results for Hartmann numbers $\text{Ha} = \sqrt{S\text{Re}_m\text{Re}}$ up to 1,000 are reported for stationary problems. Other approaches include fully-coupled geometric [1, 2] and algebraic [46, 47] monolithic multigrid methods. In [1], Adler et al. present results for a two-dimensional Hartmann problem for parameters up to $\text{Re} = \text{Re}_m = 64$.

However, the performance of most of these preconditioners deteriorates significantly for high Reynolds and coupling numbers. To the best of our knowledge, a practical robust preconditioner for the stationary MHD equations has not yet been proposed. The common problem for high magnetic Reynolds numbers and coupling numbers for the stationary case is that all available Schur complement approximations become less accurate for Newton-type linearizations, causing the linear solver to fail to converge. Conversely, Picard-type linearizations can allow an exact computation of the Schur complement but fail to converge in the nonlinear iteration.

In this work, we consider three different linearizations. The first is the Picard iteration proposed by Hu et al. [29]. We compute an approximation to the outer Schur complement of the arising block system and introduce a robust linear solver for the different blocks. This scheme works well for small magnetic Reynolds numbers but the nonlinear iteration fails to converge for higher Re_m , as anticipated in the analysis of [29]. The second is a full Newton linearization, which converges well for high Reynolds numbers and coupling numbers. However, our approximation of the Schur complement deteriorates slightly for high parameters. The third linearization scheme we analyze is novel; we call it the *minimal decoupling Picard* iteration. This only drops one term of the Newton scheme and hence provides a good nonlinear scheme in many cases, but has the advantage that the outer Schur complement can be computed exactly in two and three dimensions. As we will see in the next sections, there are many differences in the performance of the schemes between the two and three-dimensional cases.

Ma et al. [33] have developed Reynolds-robust preconditioners for the time-dependent MHD equations that are based on norm-equivalent and field-of-values equivalent approaches. To the best of our knowledge, their strategy does not extend to the stationary case; in general, the time-dependent case offers crucial advantages for the development of robust solvers. For example, Ma et al. treat complicated terms like the hydrodynamic convection term $\mathbf{u} \cdot \nabla \mathbf{u}$ explicitly in the time-stepping scheme, which can cause problems for convection-dominated problems and does not apply in

the stationary case. The discretization of the time derivative causes mass matrices with a scaling of $1/\Delta t$, where Δt denotes the time step size, to appear in the block matrix on the diagonal blocks. As we will see also in our numerical results for the time-dependent problems, these extra terms dominate the scheme for small Δt and hence simplify the development of robust solvers.

Most applications are in the regime of high Reynolds and coupling numbers and hence it is of great interest to build robust solvers with respect to these parameters. For liquid metals, the fluid Reynolds number Re tends to be much larger than Re_m . For example, the flow of liquid mercury is characterized by a ratio of 10^7 between these two constants; typical values in aluminium electrolysis are $\text{Re}_m = 10^{-1}$ and $\text{Re} = 10^5$ [25]. High magnetic Reynolds numbers occur on large length scales, as in geo- and astrophysics. The magnetic Reynolds number of the outer Earth's core is in the range of 10^3 and of the sun is in the range of 10^6 [18]. Magnetic Reynolds numbers between $10^1 - 10^3$ have been used in several dynamo experiments that investigate planetary magnetic fields [34]. The coupling number S is around 10^0 for aluminium electrolysis [25] and Armero & Simo [4] define strong coupling for S in the range of $10^2 - 10^9$.

The remainder of this work is outlined as follows. In Section 2, we derive an augmented Lagrangian formulation for (1.1) and describe the finite element discretization and linearization schemes. In Section 3, we introduce block preconditioners for these schemes, present a calculation of the corresponding (approximate) Schur complements and describe robust linear multigrid solvers for the different blocks. Numerical examples and a detailed description of the algorithm are presented in Section 4.

2. Formulation, linearization, and discretization.

2.1. An augmented Lagrangian formulation. We modify (1.1) by introducing two augmented Lagrangian terms: $-\gamma \nabla \operatorname{div} \mathbf{u}$ for $\gamma > 0$ is added to (1.1a), and $-1/\text{Re}_m \nabla \operatorname{div} \mathbf{B}$ is added to (1.1d). Note that both terms leave the continuous solution of the problem unchanged. We use the first term to control the Schur complement of the fluid subsystem [22] and the second term to enforce the divergence constraint $\operatorname{div} \mathbf{B} = 0$, as shown in [29, Thm. 9].

Following these modifications, we consider the following system

$$(2.1a) \quad -\frac{2}{\text{Re}} \operatorname{div} \varepsilon(\mathbf{u}) + \mathbf{u} \cdot \nabla \mathbf{u} - \gamma \nabla \operatorname{div} \mathbf{u} + \nabla p + S \mathbf{B} \times (\mathbf{E} + \mathbf{u} \times \mathbf{B}) = \mathbf{f},$$

$$(2.1b) \quad \operatorname{div} \mathbf{u} = 0,$$

$$(2.1c) \quad \mathbf{E} + \mathbf{u} \times \mathbf{B} - \frac{1}{\text{Re}_m} \operatorname{curl} \mathbf{B} = \mathbf{0},$$

$$(2.1d) \quad -\frac{1}{\text{Re}_m} \nabla \operatorname{div} \mathbf{B} + \operatorname{curl} \mathbf{E} = \mathbf{0},$$

subject to the boundary conditions (1.2). For convenience, we consider homogeneous boundary conditions in this section but all the results extend in a straightforward manner to inhomogeneous boundary conditions. However, there are subtle technicalities for the implementation of the degrees of freedom in the finite element method in the inhomogeneous case, which are explained in detail in Section 4.2.

The weak formulation of (2.1) seeks $\mathcal{U} := (\mathbf{u}, p, \mathbf{E}, \mathbf{B}) \in \mathcal{Z} := \mathbf{V} \times Q \times \mathbf{R} \times \mathbf{W}$ with

$$(2.2) \quad \mathbf{V} := \mathbf{H}_0^1(\Omega), \quad Q := L_0^2(\Omega), \quad \mathbf{R} := \mathbf{H}_0(\operatorname{curl}, \Omega), \quad \mathbf{W} := \mathbf{H}_0(\operatorname{div}, \Omega).$$

In two dimensions, we define $R := H_0^1(\Omega)$ which can be identified with the scalar-valued space $H_0(\operatorname{curl}, \Omega)$. The weak formulation is to find $\mathcal{U} \in \mathcal{Z}$ such that for all

$\mathcal{V} := (\mathbf{v}, q, \mathbf{F}, \mathbf{C}) \in \mathcal{Z}$ and $\mathcal{F} = (\mathbf{f}, 0, \mathbf{0}, \mathbf{0})$ there holds

$$(2.3) \quad \mathcal{N}(\mathcal{U}, \mathcal{V}) = (\mathcal{F}, \mathcal{V})$$

with

$$(2.4) \quad \begin{aligned} \mathcal{N}(\mathcal{U}, \mathcal{V}) = & \frac{2}{\text{Re}} (\varepsilon(\mathbf{u}), \varepsilon(\mathbf{v})) + (\mathbf{u} \cdot \nabla \mathbf{u}, \mathbf{v}) + \gamma(\text{div } \mathbf{u}, \text{div } \mathbf{v}) \\ & - (p, \text{div } \mathbf{v}) + S(\mathbf{B} \times \mathbf{E}, \mathbf{v}) + S(\mathbf{B} \times (\mathbf{u} \times \mathbf{B}), \mathbf{v}) \\ & - (\text{div } \mathbf{u}, q) \\ & + (\mathbf{E}, \mathbf{F}) + (\mathbf{u} \times \mathbf{B}, \mathbf{F}) - \frac{1}{\text{Re}_m} (\mathbf{B}, \text{curl } \mathbf{F}) \\ & + \frac{1}{\text{Re}_m} (\text{div } \mathbf{B}, \text{div } \mathbf{C}) + (\text{curl } \mathbf{E}, \mathbf{C}). \end{aligned}$$

All boundary integrals that result from integration by parts vanish because of the choice of the boundary conditions (1.2).

Note that \mathbf{W} and \mathbf{R} are chosen from the de Rham complex [5]

$$(2.5) \quad \mathbb{R} \xrightarrow{\text{id}} H_0^1(\Omega) \xrightarrow{\text{grad}} \mathbf{H}_0(\text{curl}, \Omega) \xrightarrow{\text{curl}} \mathbf{H}_0(\text{div}, \Omega) \xrightarrow{\text{div}} L_0^2(\Omega) \xrightarrow{\text{null}} 0,$$

which is exact for the simply connected domains we consider. The corresponding complex in two dimensions is given by

$$(2.6) \quad \mathbb{R} \xrightarrow{\text{id}} \mathbf{H}_0(\text{curl}, \Omega) \xrightarrow{\text{curl}} \mathbf{H}_0(\text{div}, \Omega) \xrightarrow{\text{div}} L_0^2(\Omega) \xrightarrow{\text{null}} 0.$$

This ensures that formulation (2.1) enforces the divergence constraint $\text{div } \mathbf{B} = 0$ and $\text{curl } \mathbf{E} = \mathbf{0}$. To see this, we test (2.3) with $\mathcal{V} = (\mathbf{0}, 0, \mathbf{0}, \text{curl } \mathbf{E})$ and conclude that $\text{curl } \mathbf{E} = \mathbf{0}$. Here, \mathcal{V} is a valid test function because the above exact sequence implies that $\text{curl}(\mathbf{R}) = \mathbf{W}$. Similarly, testing with $\mathcal{V} = (\mathbf{0}, 0, \mathbf{0}, \mathbf{B})$ results in $\text{div } \mathbf{B} = 0$.

2.2. Linearization: Newton, Picard, and minimal decoupling Picard.

The Newton linearization of (2.3) for the initial guess $\mathcal{U}^n = (\mathbf{u}^n, p^n, \mathbf{E}^n, \mathbf{B}^n)$ is to find an update $\delta\mathcal{U}$ such that

$$(2.7) \quad \mathcal{N}_N(\delta\mathcal{U}, \mathcal{U}^n, \mathcal{V}) = \mathcal{R}(\mathcal{U}^n, \mathcal{V}) \quad \forall \mathcal{V} \in \mathcal{Z},$$

$$(2.8) \quad \mathcal{U}^{n+1} = \mathcal{U}^n + \delta\mathcal{U},$$

with the weak form of the nonlinear residual $\mathcal{R}(\mathcal{U}^n, \mathcal{V})$ evaluated at \mathcal{U}^n and

$$(2.9) \quad \begin{aligned} \mathcal{N}_N(\delta\mathcal{U}, \mathcal{U}^n, \mathcal{V}) = & \frac{2}{\text{Re}} (\varepsilon(\delta\mathbf{u}), \varepsilon(\mathbf{v})) + (\mathbf{u}^n \cdot \nabla \delta\mathbf{u}, \mathbf{v}) + (\delta\mathbf{u} \cdot \nabla \mathbf{u}^n, \mathbf{v}) \\ & + \gamma(\text{div } \delta\mathbf{u}, \text{div } \mathbf{v}) - (\delta p, \text{div } \mathbf{v}) \\ & + S(\mathbf{B}^n \times \delta\mathbf{E}, \mathbf{v}) + S(\delta\mathbf{B} \times \mathbf{E}^n, \mathbf{v}) \\ & + S(\mathbf{B}^n \times (\delta\mathbf{u} \times \mathbf{B}^n), \mathbf{v}) + S(\delta\mathbf{B} \times (\mathbf{u}^n \times \mathbf{B}^n), \mathbf{v}) \\ & + S(\mathbf{B}^n \times (\mathbf{u}^n \times \delta\mathbf{B}), \mathbf{v}) \\ & - (\text{div } \delta\mathbf{u}, q) \\ & + (\delta\mathbf{E}, \mathbf{F}) + (\mathbf{u}^n \times \delta\mathbf{B}, \mathbf{F}) + (\delta\mathbf{u} \times \mathbf{B}^n, \mathbf{F}) \\ & - \frac{1}{\text{Re}_m} (\delta\mathbf{B}, \text{curl } \mathbf{F}) \\ & + \frac{1}{\text{Re}_m} (\text{div } \delta\mathbf{B}, \text{div } \mathbf{C}) + (\text{curl } \delta\mathbf{E}, \mathbf{C}). \end{aligned}$$

The bilinear form for the Picard iteration considered in [29] is given by

$$(2.10) \quad \begin{aligned} \mathcal{N}_P(\delta\mathcal{U}, \mathcal{U}^n, \mathcal{V}) = & \mathcal{N}_N(\delta\mathcal{U}, \mathcal{U}^n, \mathcal{V}) - S(\delta\mathbf{B} \times \mathbf{E}^n, \mathbf{v}) - S(\mathbf{B}^n \times (\mathbf{u}^n \times \delta\mathbf{B}), \mathbf{v}) \\ & - S(\delta\mathbf{B} \times (\mathbf{u}^n \times \mathbf{B}^n), \mathbf{v}) - (\mathbf{u}^n \times \delta\mathbf{B}, \mathbf{F}). \end{aligned}$$

Note that in contrast to [29], we do not scale the term $(\mathbf{curl} \delta\mathbf{E}, \mathbf{C})$ with S/Re_m and consider the full Newton linearization of the advection term $(\mathbf{u} \cdot \nabla)\mathbf{u}$. The advantage of this Picard linearization is that it allows an exact Schur complement computation in two dimensions and converges well for high Re . However, its major disadvantage is the failure of nonlinear convergence for high Re_m .

We now propose a new nonlinear scheme that we call the *minimal decoupling Picard* (MDP) iteration, which eliminates only the term $(\delta\mathbf{u} \times \mathbf{B}^n, \mathbf{F})$ from the Newton form, i.e.,

$$(2.11) \quad \mathcal{N}_{MDP}(\delta\mathcal{U}, \mathcal{U}^n, \mathcal{V}) = \mathcal{N}_N(\delta\mathcal{U}, \mathcal{U}^n, \mathcal{V}) - (\delta\mathbf{u} \times \mathbf{B}^n, \mathbf{F}).$$

As we show later, the advantage of this scheme is that we are able to control the Schur complement of the linear system while the nonlinear scheme still converges well in many (but not all) cases.

2.3. Discretization. For a finite element discretization, we seek $\mathcal{U}_h := (\mathbf{u}_h, p_h, \mathbf{E}_h, \mathbf{B}_h) \in \mathcal{Z}_h := \mathbf{V}_h \times Q_h \times \mathbf{R}_h \times \mathbf{W}_h$ such that

$$(2.12) \quad \mathcal{N}(\mathcal{U}_h, \mathcal{V}_h) = (\mathcal{F}, \mathcal{V}_h) \quad \forall \mathcal{V}_h \in \mathcal{Z}_h.$$

We choose Raviart–Thomas elements of degree k \mathbb{RT}_k [41] for \mathbf{W}_h , Nédélec elements of first kind $\mathbb{NED}1_k$ [35] for \mathbf{R}_h in 3D and continuous Lagrange elements \mathbb{CG}_k for R_h in 2D. Note that these elements belong to a discrete subcomplex of (2.5)

$$(2.13) \quad \mathbb{CG}_k \xrightarrow{\text{grad}} \mathbb{NED}1_k \xrightarrow{\mathbf{curl}} \mathbb{RT}_k \xrightarrow{\text{div}} \mathbb{DG}_{k-1} \xrightarrow{\text{null}} 0,$$

and of (2.6)

$$(2.14) \quad \mathbb{CG}_k \xrightarrow{\mathbf{curl}} \mathbb{RT}_k \xrightarrow{\text{div}} \mathbb{DG}_{k-1} \xrightarrow{\text{null}} 0.$$

This implies that we enforce $\text{div } \mathbf{B}_h = 0$ and $\mathbf{curl} \mathbf{E}_h = \mathbf{0}$ pointwise with the same proof as for the continuous case. These identities also hold for inhomogeneous boundary conditions, since the interpolation operator $\mathcal{I}_{\mathbf{W}_h}^h$ into the Raviart–Thomas space satisfies for all divergence-free $\mathbf{B} \in \mathbf{H}_0(\text{div}, \Omega)$ [10, Prop. 2.5.2]

$$(2.15) \quad \text{div}(\mathcal{I}_{\mathbf{W}_h}^h \mathbf{B}) = 0.$$

Moreover, following [19], we add the following stabilization term to address the problem that the Galerkin discretization of advection-dominated problems can be oscillatory [20]

$$(2.16) \quad \mathcal{ST}(\mathbf{u}_h, \mathbf{v}_h) = \sum_{K \in \mathcal{M}_h} \frac{1}{2} \int_{\partial K} \mu h_{\partial K}^2 [\![\nabla \mathbf{u}_h]\!] : [\![\nabla \mathbf{v}_h]\!] \, ds.$$

Here, $[\![\nabla \mathbf{u}_h]\!]$ denotes the jump of the gradient, $h_{\partial K}$ is a function giving the facet size, and μ is a free parameter that is chosen according to [13].

Note that a fully robust discretization should also include a stabilization term for the magnetic field \mathbf{B} in the case of dominating magnetic advection. The literature

does not propose many stabilization types for this problem. The most promising work by Wu and Xu [50] uses the so-called SAFE-scheme for stabilization which is based on an exponential fitting approach. While the original SAFE-scheme is only a first order method, it can be extended to higher order as shown in [51]. We aim to include this stabilization in future work.

For the hydrodynamic part, we consider the $\mathbf{H}(\text{div}) \times L^2$ -conforming element pair $\mathbb{BDM}_k \times \mathbb{DG}_{k-1}$ with the Brezzi-Douglas-Marini element \mathbb{BDM}_k of order k [12, 36]. This discretization ensures that $\text{div } \mathbf{u}_h = 0$ holds pointwise [31] since $\text{div } \mathbf{V}_h \subset Q_h$. Additionally, it exhibits pressure robustness, i.e. the error estimates do not degrade for high Reynolds numbers.

Since the discretization is nonconforming, we must consider a discontinuous Galerkin formulation of the hydrodynamic advection and diffusion terms [24, section 7]. We denote by $\mathcal{F}_h = \mathcal{F}_h^i \cup \mathcal{F}_h^\partial$ all facets of the triangulation, which consists of the interior facets \mathcal{F}_h^i and the Dirichlet boundary facets \mathcal{F}_h^∂ . We assign to each $F \in \mathcal{F}_h$ its diameter h_F and unit normal vector \mathbf{n}_F . The jump and average operators across a facet are denoted by $[\![\cdot]\!]$ and $\{\!\{\cdot\}\!\}$ respectively and are defined as $[\![\Phi]\!] = \Phi^+ - \Phi^-$ and $\{\!\{\Phi\}\!\} = \frac{1}{2}(\Phi^+ + \Phi^-)$. The penalization parameter is chosen as $\sigma = 10k^2$. Inhomogeneous boundary data are described by \mathbf{g}_D . We then add the following bilinear forms to (2.12):

$$\begin{aligned}
a_h^{DG}(\mathbf{u}_h, \mathbf{v}_h) = & -\frac{2}{\text{Re}} \sum_{F \in \mathcal{F}_h} \int_F \{\!\{\varepsilon(\mathbf{u}_h)\}\!\} \mathbf{n}_F \cdot [\![\mathbf{v}_h]\!] \, ds \\
& -\frac{2}{\text{Re}} \sum_{F \in \mathcal{F}_h} \int_F [\![\mathbf{u}_h]\!] \cdot \{\!\{\varepsilon(\mathbf{v}_h)\}\!\} \mathbf{n}_F \, ds \\
& + \frac{1}{\text{Re}} \sum_{F \in \mathcal{F}_h} \frac{\sigma}{h_F} \int_F [\![\mathbf{u}_h]\!] \cdot [\![\mathbf{v}_h]\!] \, ds \\
& -\frac{1}{\text{Re}} \sum_{F \in \mathcal{F}_h^\partial} \frac{\sigma}{h_F} \int_F \mathbf{g}_D \cdot \mathbf{v}_h \, ds + \frac{2}{\text{Re}} \sum_{F \in \mathcal{F}_h^\partial} \int_F \mathbf{g}_D \cdot \varepsilon(\mathbf{v}_h) \mathbf{n}_F \, ds, \\
c_h^{DG}(\mathbf{u}_h, \mathbf{v}_h) = & \frac{1}{2} \sum_{F \in \mathcal{F}_h^i} \int_F [\![(\mathbf{u}_h \cdot \mathbf{n}_F + |\mathbf{u}_h \cdot \mathbf{n}_F|)\mathbf{u}_h]\!] \cdot [\![\mathbf{v}_h]\!] \, ds \\
& + \frac{1}{2} \sum_{F \in \mathcal{F}_h^\partial} \int_F (\mathbf{u}_h \cdot \mathbf{n}_F + |\mathbf{u}_h \cdot \mathbf{n}_F|) \mathbf{u}_h \cdot \mathbf{v}_h \, ds \\
& + \frac{1}{2} \sum_{F \in \mathcal{F}_h^\partial} \int_F (\mathbf{u}_h \cdot \mathbf{n}_F - |\mathbf{u}_h \cdot \mathbf{n}_F|) \mathbf{g}_D \cdot \mathbf{v}_h \, ds.
\end{aligned}
\tag{2.17, 2.18}$$

Hu et al. prove in [29, Theorem 4] that (2.12) is well-posed and has at least one solution. The solution is unique for suitable source and boundary data. While the well-posedness and convergence of the Newton and minimal decoupling Picard iterations remain open problems, Hu et al. prove that the Picard iteration converges to the unique solution of (2.12) if both $\text{Re}^2 \|f\|_{-1}$ and $\text{Re} \text{Re}_m^{\frac{3}{2}} \|f\|_{-1}$ are small enough.

For the Newton linearization (2.9), we must solve the following linear system at

each step:

$$(2.19) \quad \begin{bmatrix} \mathcal{F} + \mathcal{D} & \mathcal{B}^\top & \mathcal{J} & \tilde{\mathcal{J}} + \tilde{\mathcal{D}}_1 + \tilde{\mathcal{D}}_2 \\ \mathcal{B} & \mathbf{0} & \mathbf{0} & \mathbf{0} \\ \mathcal{G} & \mathbf{0} & \mathcal{M}_{\mathbf{E}} & \tilde{\mathcal{G}} - \frac{1}{\text{Re}_m} \mathcal{A} \\ \mathbf{0} & \mathbf{0} & \mathcal{A}^\top & \frac{1}{\text{Re}_m} \mathcal{C} \end{bmatrix} \begin{bmatrix} x_{\mathbf{u}} \\ x_p \\ x_{\mathbf{E}} \\ x_{\mathbf{B}} \end{bmatrix} = \begin{bmatrix} R_{\mathbf{u}} \\ R_p \\ R_{\mathbf{E}} \\ R_{\mathbf{B}} \end{bmatrix},$$

where $x_{\mathbf{u}}$, x_p , $x_{\mathbf{E}}$ and $x_{\mathbf{B}}$ are the coefficients of the discretized Newton corrections and $R_{\mathbf{u}}$, R_p , $R_{\mathbf{E}}$ and $R_{\mathbf{B}}$ the corresponding nonlinear residuals. The correspondence between the discrete and continuous operators is illustrated in Table 2.1. We have chosen the notation that operators that include a tilde are omitted in the Picard linearization (2.10). Only the matrix \mathcal{G} is dropped for the minimal decoupling Picard linearization (2.11), which is the minimal change that renders the matrix block-upper-triangular.

Discrete	Continuous	Weak form
$\mathcal{F}\mathbf{u}$	$-\frac{2}{\text{Re}} \operatorname{div} \varepsilon(\mathbf{u}) + \mathbf{u}^n \cdot \nabla \mathbf{u} + \mathbf{u} \cdot \nabla \mathbf{u}^n$ $-\gamma \nabla \operatorname{div} \mathbf{u}$	$\frac{2}{\text{Re}} (\varepsilon(\mathbf{u}), \varepsilon(\mathbf{v})) + (\mathbf{u}^n \cdot \nabla \mathbf{u}, \mathbf{v})$ $+ (\mathbf{u} \cdot \nabla \mathbf{u}^n, \mathbf{v}) + \gamma (\operatorname{div} \mathbf{u}, \operatorname{div} \mathbf{v})$
$\mathcal{D}\mathbf{u}$	$S\mathbf{B}^n \times (\mathbf{u} \times \mathbf{B}^n)$	$S(\mathbf{B}^n \times (\mathbf{u} \times \mathbf{B}^n), \mathbf{v})$
$\mathcal{J}\mathbf{E}$	$S\mathbf{B}^n \times \mathbf{E}$	$S(\mathbf{B}^n \times \mathbf{E}, \mathbf{v})$
$\tilde{\mathcal{J}}\mathbf{B}$	$S\mathbf{B} \times \mathbf{E}^n$	$S(\mathbf{B} \times \mathbf{E}^n, \mathbf{v})$
$\tilde{\mathcal{D}}_1\mathbf{B}$	$S\mathbf{B} \times (\mathbf{u}^n \times \mathbf{B}^n)$	$S(\mathbf{B} \times (\mathbf{u}^n \times \mathbf{B}^n), \mathbf{v})$
$\tilde{\mathcal{D}}_2\mathbf{B}$	$S\mathbf{B}^n \times (\mathbf{u}^n \times \mathbf{B})$	$S(\mathbf{B}^n \times (\mathbf{u}^n \times \mathbf{B}), \mathbf{v})$
$\mathcal{M}_{\mathbf{E}}\mathbf{E}$	\mathbf{E}	(\mathbf{E}, \mathbf{F})
$\mathcal{G}\mathbf{u}$	$\mathbf{u} \times \mathbf{B}^n$	$(\mathbf{u} \times \mathbf{B}^n, \mathbf{F})$
$\tilde{\mathcal{G}}\mathbf{B}$	$\mathbf{u}^n \times \mathbf{B}$	$(\mathbf{u}^n \times \mathbf{B}, \mathbf{F})$
$\mathcal{A}\mathbf{B}$	$\operatorname{curl} \mathbf{B}$	$(\mathbf{B}, \operatorname{curl} \mathbf{F})$
$\mathcal{C}\mathbf{B}$	$-\nabla \operatorname{div} \mathbf{B}$	$(\operatorname{div} \mathbf{B}, \operatorname{div} \mathbf{C})$
$\mathcal{A}^\top\mathbf{E}$	$\operatorname{curl} \mathbf{E}$	$(\operatorname{curl} \mathbf{E}, \mathbf{C})$
$\mathcal{B}^\top p$	∇p	$-(p, \operatorname{div} \mathbf{v})$
$\mathcal{B}\mathbf{u}$	$-\operatorname{div} \mathbf{u}$	$-(\operatorname{div} \mathbf{u}, q)$

Table 2.1: Overview of operators.

3. Derivation of block preconditioners. We now consider block preconditioners for (2.19). In Section 3.1 and 3.2 we derive approximations of the Schur complements for two different block elimination strategies. Since these approximations differ for the three linearization schemes in two and three dimensions, we provide a summary in Table 3.1. We then describe the multigrid methods that we use to solve the top-left block and the Schur complement approximations in Section 3.4 and 3.5.

Both block preconditioners we consider gather the variables as $(\mathbf{E}_h, \mathbf{B}_h)$ and (\mathbf{u}_h, p_h) . They differ in the order of block elimination: the first takes the Schur complement that eliminates (inverts) the $(\mathbf{E}_h, \mathbf{B}_h)$ block, while the second takes the Schur complement that eliminates the (\mathbf{u}_h, p_h) block. The first choice appears several times in the literature [32, 39], while it seems that the second choice has not yet been investigated. As we will see, for small Re_m and S both preconditioners perform similarly, while for more difficult parameter regimes the second choice notably outperforms the first. We therefore recommend the second strategy and mainly report

numerical results for this choice. Nevertheless, we also investigate the first option, both for comparison and because it allows a much more detailed description of the outer Schur complement. In two dimensions it even allows an exact computation of the Schur complement. The two strategies are compared in Section 4.4.2 below.

For the time-dependent equations, we concentrate here on the implicit Euler method, but the following computations are straightforward to adapt to other implicit multi-step methods. For implicit Euler, the expression $\frac{1}{\Delta t}(\mathbf{u}, \mathbf{v})$ is added to \mathcal{F} and $\frac{1}{\Delta t}(\mathbf{B}, \mathbf{C})$ to \mathcal{C} . Note that in the transient case, the equation

$$(3.1) \quad \partial_t \mathbf{B} + \mathbf{curl} \mathbf{E} = \mathbf{0}$$

immediately implies $\operatorname{div} \mathbf{B} = 0$ if the initial condition satisfies $\operatorname{div} \mathbf{B}_0 = 0$, and this remains true on the discrete level [28]. Hence, the augmented Lagrangian term $-\frac{1}{\operatorname{Re}_m} \nabla \operatorname{div} \mathbf{B}$ is no longer necessary to enforce the divergence constraint and could therefore be omitted. Nevertheless, we retain it in our scheme since we employ the identity

$$(3.2) \quad \frac{1}{\operatorname{Re}_m} \mathbf{curl} \mathbf{curl} \mathbf{u} - \frac{1}{\operatorname{Re}_m} \nabla \operatorname{div} \mathbf{u} = -\frac{1}{\operatorname{Re}_m} \Delta \mathbf{u}$$

in our derivation of Schur complement approximations below.

3.1. Outer Schur complement eliminating the $(\mathbf{E}_h, \mathbf{B}_h)$ block. Reordering (2.19) for convenience, we consider

$$(3.3) \quad \left[\begin{array}{cc|cc} \mathcal{M}_{\mathbf{E}} & \tilde{\mathcal{G}} - \frac{1}{\operatorname{Re}_m} \mathcal{A} & \mathcal{G} & \mathbf{0} \\ \mathcal{A}^\top & \frac{1}{\operatorname{Re}_m} \mathcal{C} & \mathbf{0} & \mathbf{0} \\ \hline \mathcal{J} & \tilde{\mathcal{J}} + \tilde{\mathcal{D}}_1 + \tilde{\mathcal{D}}_2 & \mathcal{F} + \mathcal{D} & \mathcal{B}^\top \\ \mathbf{0} & \mathbf{0} & \mathcal{B} & \mathbf{0} \end{array} \right] \begin{bmatrix} x_{\mathbf{E}} \\ x_{\mathbf{B}} \\ x_{\mathbf{u}} \\ x_p \end{bmatrix} = \begin{bmatrix} R_{\mathbf{E}} \\ R_{\mathbf{B}} \\ R_{\mathbf{u}} \\ R_p \end{bmatrix}.$$

The outer Schur complement eliminating the $(\mathbf{E}_h, \mathbf{B}_h)$ block is given by

$$(3.4) \quad \mathcal{S}_N^{(\mathbf{E}, \mathbf{B})} = \begin{bmatrix} \mathcal{F} + \mathcal{D} & \mathcal{B}^\top \\ \mathcal{B} & \mathbf{0} \end{bmatrix} - \begin{bmatrix} \mathcal{J} & \tilde{\mathcal{J}} + \tilde{\mathcal{D}}_1 + \tilde{\mathcal{D}}_2 \\ \mathbf{0} & \mathbf{0} \end{bmatrix} \begin{bmatrix} \mathcal{M}_{\mathbf{E}} & \tilde{\mathcal{G}} - \frac{1}{\operatorname{Re}_m} \mathcal{A} \\ \mathcal{A}^\top & \frac{1}{\operatorname{Re}_m} \mathcal{C} \end{bmatrix}^{-1} \begin{bmatrix} \mathcal{G} & \mathbf{0} \\ \mathbf{0} & \mathbf{0} \end{bmatrix}.$$

We immediately see that, for the minimal decoupling Picard linearization that omits the matrix \mathcal{G} , the Schur complement simplifies to

$$(3.5) \quad \mathcal{S}_{MDP}^{(\mathbf{E}, \mathbf{B})} = \begin{bmatrix} \mathcal{F} + \mathcal{D} & \mathcal{B}^\top \\ \mathcal{B} & \mathbf{0} \end{bmatrix},$$

i.e. the Navier–Stokes block with the linearized Lorentz force. For the Newton linearization, we simplify $\mathcal{S}_N^{(\mathbf{E}, \mathbf{B})}$ using the identity

$$(3.6) \quad \begin{bmatrix} \mathcal{A} & \mathcal{B} \\ \mathcal{C} & \mathcal{D} \end{bmatrix}^{-1} = \begin{bmatrix} \mathcal{A}^{-1} + \mathcal{A}^{-1} \mathcal{B} (\mathcal{D} - \mathcal{C} \mathcal{A}^{-1} \mathcal{B})^{-1} \mathcal{C} \mathcal{A}^{-1} & -\mathcal{A}^{-1} \mathcal{B} (\mathcal{D} - \mathcal{C} \mathcal{A}^{-1} \mathcal{B})^{-1} \\ -(\mathcal{D} - \mathcal{C} \mathcal{A}^{-1} \mathcal{B})^{-1} \mathcal{C} \mathcal{A}^{-1} & (\mathcal{D} - \mathcal{C} \mathcal{A}^{-1} \mathcal{B})^{-1} \end{bmatrix}$$

for non-singular matrices \mathcal{A} and $\mathcal{D} - \mathcal{C} \mathcal{A}^{-1} \mathcal{B}$. We apply this formula to the top-left electromagnetic block

$$(3.7) \quad \mathcal{M} = \begin{bmatrix} \mathcal{M}_{\mathbf{E}} & \tilde{\mathcal{G}} - \frac{1}{\operatorname{Re}_m} \mathcal{A} \\ \mathcal{A}^\top & \frac{1}{\operatorname{Re}_m} \mathcal{C} \end{bmatrix}.$$

This results in

$$(3.8) \quad \mathcal{S}_N^{(\mathbf{E}, \mathbf{B})} = \begin{bmatrix} \mathcal{F} + \mathcal{D} - \mathcal{J}\mathcal{M}_{1,1}^{-1}\mathcal{G} - (\tilde{\mathcal{J}} + \tilde{\mathcal{D}}_1 + \tilde{\mathcal{D}}_2)\mathcal{M}_{2,1}^{-1}\mathcal{G} & \mathcal{B}^\top \\ \mathcal{B} & \mathbf{0} \end{bmatrix}$$

with

$$(3.9) \quad \mathcal{M}_{1,1}^{-1} = \mathcal{M}_{\mathbf{E}}^{-1} + \mathcal{M}_{\mathbf{E}}^{-1} \left(\tilde{\mathcal{G}} - \frac{1}{\text{Re}_m} \mathcal{A} \right) \left(\frac{1}{\text{Re}_m} \mathcal{C} - \mathcal{A}^\top \mathcal{M}_{\mathbf{E}}^{-1} \left(\tilde{\mathcal{G}} - \frac{1}{\text{Re}_m} \mathcal{A} \right) \right)^{-1} \mathcal{A}^\top \mathcal{M}_{\mathbf{E}}^{-1}$$

and

$$(3.10) \quad \mathcal{M}_{2,1}^{-1} = - \left(\frac{1}{\text{Re}_m} \mathcal{C} - \mathcal{A}^\top \mathcal{M}_{\mathbf{E}}^{-1} \left(\tilde{\mathcal{G}} - \frac{1}{\text{Re}_m} \mathcal{A} \right) \right)^{-1} \mathcal{A}^\top \mathcal{M}_{\mathbf{E}}^{-1}.$$

In the following, we compute approximations to the outer Schur complement for the Picard and Newton linearizations. We mainly follow [39], but adapt the computations for our formulation which includes the electric field \mathbf{E} instead of a Lagrange multiplier r .

For the simplification of the outer Schur complement $\mathcal{S}_N^{(\mathbf{E}, \mathbf{B})}$ we must find approximations for

$$(3.11) \quad \mathcal{D} - \mathcal{J}\mathcal{M}_{1,1}^{-1}\mathcal{G} \quad \text{and} \quad -(\tilde{\mathcal{J}} + \tilde{\mathcal{D}}_1 + \tilde{\mathcal{D}}_2)\mathcal{M}_{2,1}^{-1}\mathcal{G}.$$

Note that the first summand of $\mathcal{J}\mathcal{M}_{1,1}^{-1}\mathcal{G}$ is $\mathcal{J}\mathcal{M}_{\mathbf{E}}^{-1}\mathcal{G}$ which equals \mathcal{D} . Hence, it remains to find an approximation to the second summand

$$(3.12) \quad -\mathcal{J}\mathcal{M}_{\mathbf{E}}^{-1} \left(\tilde{\mathcal{G}} - \frac{1}{\text{Re}_m} \mathcal{A} \right) \left(\frac{1}{\text{Re}_m} \mathcal{C} - \mathcal{A}^\top \mathcal{M}_{\mathbf{E}}^{-1} \left(\tilde{\mathcal{G}} - \frac{1}{\text{Re}_m} \mathcal{A} \right) \right)^{-1} \mathcal{A}^\top \mathcal{M}_{\mathbf{E}}^{-1}\mathcal{G}$$

which corresponds on a continuous level to

$$(3.13) \quad -S \mathbf{B}^n \times \left(\left(\delta \mathbf{u}^n \times \cdot - \frac{1}{\text{Re}_m} \mathbf{curl} \right) \left(\frac{\eta}{\Delta t} I - \frac{1}{\text{Re}_m} \Delta - \delta \mathbf{curl}(\mathbf{u}^n \times \cdot) \right)^{-1} \mathbf{curl}(\mathbf{u} \times \mathbf{B}^n) \right).$$

The continuous expression for $-(\tilde{\mathcal{J}} + \tilde{\mathcal{D}}_1 + \tilde{\mathcal{D}}_2)\mathcal{M}_{2,1}^{-1}\mathcal{G}$ is given by

$$(3.14) \quad \begin{aligned} & \delta S (\cdot \times \mathbf{E}^n + \cdot \times (\mathbf{u}^n \times \mathbf{B}^n) + \mathbf{B}^n \times (\mathbf{u}^n \times \cdot)) \\ & \left(\frac{\eta}{\Delta t} I - \frac{1}{\text{Re}_m} \Delta - \mathbf{curl}(\mathbf{u}^n \times \cdot) \right)^{-1} \mathbf{curl}(\mathbf{u} \times \mathbf{B}^n). \end{aligned}$$

Here, we have used $\eta, \delta \in \{0, 1\}$ to distinguish between the stationary ($\eta = 0$) and transient ($\eta = 1$) cases and between the Picard ($\delta = 0$) and Newton ($\delta = 1$) linearization.

3.1.1. The two-dimensional case. For the Picard linearization, expression (3.12) simplifies to \mathcal{D} in the stationary case. This follows immediately from the two-dimensional analogue of (3.2) and the identity [38]

$$(3.15) \quad \mathbf{curl}(-\Delta)^{-1} \mathbf{curl} \varphi = \varphi$$

which implies for our structure-preserving discretization that

$$(3.16) \quad \mathcal{A}(\mathcal{C} + \mathcal{A}^\top \mathcal{M}_{\mathbf{E}}^{-1} \mathcal{A})^{-1} \mathcal{A}^\top = \mathcal{M}_{\mathbf{E}}.$$

That means in the two-dimensional stationary case the outer Schur complement for the Picard iteration $\mathcal{S}_P^{(\mathbf{E}, \mathbf{B})}$ is given by $\mathcal{S}_{MDP}^{(\mathbf{E}, \mathbf{B})}$.

In the transient case the Schur complement for the Picard linearization can no longer be calculated exactly. The behavior of the Schur complement now depends on which of the terms $\frac{1}{\Delta t}I$ and $\frac{1}{Re_m}\Delta$ dominates. If $\frac{h^2}{\Delta t}$ is small in comparison to $\frac{1}{Re_m}$, a good approximation of (3.12) is given, as in the stationary case, by $\mathcal{S}_{MDP}^{(\mathbf{E}, \mathbf{B})}$. If $\frac{1}{\Delta t}I$ dominates, the magnitude of (3.12) is given by $\frac{S\|\mathbf{B}^n\|^2\Delta t}{Re_m h^2} \ll 1$ and can therefore be neglected. We use the approximation of Phillips et al. [39] who suggest to use

$$(3.17) \quad \mathcal{S}_{MDP,\alpha}^{(\mathbf{E}, \mathbf{B})} := \begin{bmatrix} \mathcal{F} + \alpha\mathcal{D} & \mathcal{B}^\top \\ \mathcal{B} & \mathbf{0} \end{bmatrix}, \quad \alpha = \frac{\Delta t}{\Delta t + Re_m h^2 + \delta Re_m h \|\mathbf{u}^n\|_{L^2} \Delta t}$$

to address these two cases.

A simplification for $\mathcal{S}_N^{(\mathbf{E}, \mathbf{B})}$ is not straightforward, but our numerical tests suggest that $\mathcal{S}_{MDP}^{(\mathbf{E}, \mathbf{B})}$ and $\mathcal{S}_{MDP,\alpha}^{(\mathbf{E}, \mathbf{B})}$ are acceptable preconditioners for $\mathcal{S}_N^{(\mathbf{E}, \mathbf{B})}$ in the stationary and transient cases, deteriorating only for high S and Re_m . This can be explained by the fact that for small Re_m or Δt the term $\frac{\eta}{\Delta t}I - \frac{1}{Re_m}\Delta$ dominates the scheme, while for large S the missing terms in (3.13) and (3.14) gain more influence.

3.1.2. The three dimensional case. The main difficulty in three dimensions is that the identity (3.15) no longer holds. Therefore, $\mathcal{S}_{MDP}^{(\mathbf{E}, \mathbf{B})}$ is not the exact outer Schur complement for the Picard linearization in the stationary case. In [39] the same approximation from the two dimensional case is used in three dimensions. Based on the previous analysis, we expect this approximation to work well when the term Δt dominates and to deteriorate in the other cases, especially in the stationary case. The three dimensional performance of this preconditioner could be substantially improved with a better approximation of $\mathbf{curl}\Delta^{-1}\mathbf{curl}$ than a scaled identity.

We briefly comment on the main part of the outer Schur complement in the stationary case, given by

$$(3.18) \quad S\mathbf{B}^n \times [\mathbf{curl}\Delta^{-1}\mathbf{curl}(\mathbf{u} \times \mathbf{B}^n)].$$

As shown in [37, Chapter 4] one can rewrite $\mathbf{curl}\Delta^{-1}\mathbf{curl}$ as $I - \nabla\Delta_r^{-1}\operatorname{div}$, where Δ_r denotes a scalar Laplacian. These two representations show that the operator is the identity on divergence-free functions and maps curl-free functions to zero. Hence, this operator corresponds to the orthogonal L^2 -projection of a vector field onto its divergence-free part, which we denote by \mathbb{P} . Thus, the weak form of (3.18) is given by

$$(3.19) \quad S(\mathbb{P}(\mathbf{u} \times \mathbf{B}^n), \mathbb{P}(\mathbf{v} \times \mathbf{B}^n)).$$

The key challenge is then to find a sparse approximation of (3.19). We do not further address this challenge here and focus instead on the outer Schur complement that eliminates the (\mathbf{u}_h, p_h) block.

We summarize the outer Schur complement approximations for the different linearizations in Table 3.1.

3.2. Outer Schur complement eliminating the (\mathbf{u}_h, p_h) block. The outer Schur complement eliminating the (\mathbf{u}_h, p_h) is given by

$$(3.20) \quad \mathcal{S}_N^{(\mathbf{u}, p)} = \begin{bmatrix} \mathcal{M}_{\mathbf{E}} & \tilde{\mathcal{G}} - \frac{1}{Re_m}\mathcal{A} \\ \mathcal{A}^\top & \frac{1}{Re_m}\mathcal{C} \end{bmatrix} - \begin{bmatrix} \mathcal{G} & \mathbf{0} \\ \mathbf{0} & \mathbf{0} \end{bmatrix} \begin{bmatrix} \mathcal{F} + \mathcal{D} & \mathcal{B}^\top \\ \mathcal{B} & \mathbf{0} \end{bmatrix}^{-1} \begin{bmatrix} \mathcal{J} & \tilde{\mathcal{J}} + \tilde{\mathcal{D}}_1 + \tilde{\mathcal{D}}_2 \\ \mathbf{0} & \mathbf{0} \end{bmatrix}.$$

	Picard	MDP	Newton
Stationary	$\mathcal{S}_{\text{MDP}}^{(\mathbf{E}, \mathbf{B})}(\checkmark, \times)$	$\mathcal{S}_{\text{MDP}}^{(\mathbf{E}, \mathbf{B})}(\checkmark, \checkmark)$	$\mathcal{S}_{\text{MDP}}^{(\mathbf{E}, \mathbf{B})}(\times, \times)$
Transient	$\mathcal{S}_{\text{MDP}, \alpha}^{(\mathbf{E}, \mathbf{B})}(\times, \times)$	$\mathcal{S}_{\text{MDP}}^{(\mathbf{E}, \mathbf{B})}(\checkmark, \checkmark)$	$\mathcal{S}_{\text{MDP}, \alpha}^{(\mathbf{E}, \mathbf{B})}(\times, \times)$

Table 3.1: Outer Schur complement approximations for taking the Schur complement that eliminates the $(\mathbf{E}_h, \mathbf{B}_h)$ block. Entries in brackets indicate whether the approximation is exact in two and three dimensions.

Formula (3.6) implies that the outer Schur complement for the Newton iteration is given by

$$(3.21) \quad \mathcal{S}_{\text{N}}^{(\mathbf{u}, p)} = \begin{bmatrix} \mathcal{M}_{\mathbf{E}} - \mathcal{G}\mathcal{M}_{1,1}^{-1}\mathcal{J} & \tilde{\mathcal{G}} - \frac{1}{\text{Re}_m}\mathcal{A} - \mathcal{G}\mathcal{M}_{1,1}^{-1}(\tilde{\mathcal{J}} + \tilde{\mathcal{D}}_1 + \tilde{\mathcal{D}}_2) \\ \mathcal{A}^\top & \frac{1}{\text{Re}_m}\mathcal{C} \end{bmatrix},$$

where

$$(3.22) \quad \mathcal{M}_{1,1}^{-1} = (\mathcal{F} + \mathcal{D})^{-1} - (\mathcal{F} + \mathcal{D})^{-1}\mathcal{B}^\top(-\mathcal{B}(\mathcal{F} + \mathcal{D})^{-1}\mathcal{B}^\top)^{-1}\mathcal{B}(\mathcal{F} + \mathcal{D})^{-1}.$$

Similar to the other order of elimination, the outer Schur complement for the minimal decoupling Picard iteration simplifies to

$$(3.23) \quad \mathcal{S}_{\text{MDP}}^{(\mathbf{u}, p)} = \begin{bmatrix} \mathcal{M}_{\mathbf{E}} & \tilde{\mathcal{G}} - \frac{1}{\text{Re}_m}\mathcal{A} \\ \mathcal{A}^\top & \frac{1}{\text{Re}_m}\mathcal{C} \end{bmatrix}.$$

However, for this strategy, further simplifications of the Picard or Newton linearizations are not straightforward. Our numerical results in the next section show that $\mathcal{S}_{\text{MDP}}^{(\mathbf{u}, p)}$ works very well as a preconditioner for both schemes. Indeed, in contrast to the previous other order of elimination, this approximation works qualitatively the same in two and three dimensions. In theory, the approximation should deteriorate in the stationary case for very high Re_m , which we also observe numerically. However, control of the outer Schur complement is maintained for high coupling numbers S , which will clearly be seen in our numerical results in Section 4.4.2 below. This behavior is perhaps explained by the fact that $\mathcal{M}_{1,1}^{-1}$ also includes a factor S in the inverse of $(\mathcal{F} + \mathcal{D})$, which cancels the factor of S in the matrices \mathcal{J} , $\tilde{\mathcal{J}}$, $\tilde{\mathcal{D}}_1$ and $\tilde{\mathcal{D}}_2$.

To use these block preconditioners in practice, we must develop robust preconditioners for the electromagnetic and hydrodynamic subsystems.

3.3. Robust multigrid methods for the hydrodynamic and electromagnetic blocks. The equations we wish to solve become nearly singular in the parameter regimes of interest at high Reynolds and coupling numbers. Standard multigrid methods are known to perform poorly for these kinds of problems. The key components for a robust multigrid method for nearly singular problems are a parameter-robust relaxation method, that efficiently damps error modes in the kernel of the singular operators, and a kernel-preserving prolongation operator, as revealed in the seminal work of Schöberl [43].

A recent summary of the theory of robust relaxation methods can be found in [21]. Briefly, we consider the multigrid relaxation methods in the framework of subspace correction methods [52]. These decompose the (finite-dimensional) trial space V as

$$(3.24) \quad V = \sum_i V_i,$$

where the sum is not necessarily direct. A rigorous statement regarding the properties this decomposition (3.24) must fulfil to yield a robust relaxation method can be found in [43, Theorem 4.1]. A key property is that the kernel \mathcal{N} of the positive-semidefinite terms is decomposed over the subspaces, i.e.,

$$(3.25) \quad \mathcal{N} = \sum_i (V_i \cap \mathcal{N}).$$

This property means that it must be possible to write any kernel function as the sum of kernel functions in the subspaces V_i . This implies that the subspaces V_i must be at least rich enough to support nonzero kernel functions. The choice of the space decomposition (3.24) is often made by consideration of the discrete Hilbert complexes underpinning the discretization.

3.4. Solver for the hydrodynamic block. In the following, we describe a fluid Reynolds-robust preconditioner for the hydrodynamic (\mathbf{u}_h, p_h) block corresponding to

$$(3.26) \quad \begin{aligned} \frac{2}{\text{Re}} (\varepsilon(\mathbf{u}), \varepsilon(\mathbf{v})) + (\mathbf{u}^n \cdot \nabla \mathbf{u}, \mathbf{v}) + (\mathbf{u} \cdot \nabla \mathbf{u}^n, \mathbf{v}) + \gamma(\text{div } \mathbf{u}, \text{div } \mathbf{v}) \\ + S(\mathbf{B}^n \times (\mathbf{u} \times \mathbf{B}^n), \mathbf{v}) - (p, \text{div } \mathbf{v}) = (\mathbf{f}, \mathbf{v}) \quad \forall \mathbf{v} \in \mathbf{H}_0^1(\Omega), \\ -(\text{div } \mathbf{u}, q) = 0 \quad \forall q \in L^2(\Omega). \end{aligned}$$

This block corresponds to the standard Newton linearization of the Navier–Stokes equations with an augmented Lagrangian term, plus the linearization of the Lorentz force \mathcal{D} . We follow the approach of [27, 23, 22] to solve this system. The first idea is to use the augmented Lagrangian term $-\gamma \nabla \text{div } \mathbf{u}$ to control the inner Schur complement of the hydrodynamic block by choosing a large γ , e.g. $\gamma \approx 10^4$. One can show that the inner Schur complement of the augmented system $\tilde{\mathcal{S}}_{\text{NS}}$ satisfies

$$(3.27) \quad \tilde{\mathcal{S}}_{\text{NS}}^{-1} = \mathcal{S}_{\text{NS}}^{-1} - \gamma \mathcal{M}_p^{-1}$$

where $\mathcal{S}_{\text{NS}}^{-1}$ denotes the Schur complement of the system without the augmented Lagrangian term and \mathcal{M}_p denotes the pressure mass matrix. Therefore, for large γ the pressure mass matrix scaled by $-(1/\text{Re} + \gamma)$ is a good approximation for $\tilde{\mathcal{S}}$. As the discretization considered in this work uses discontinuous pressures, the pressure mass matrix is block-diagonal and hence directly invertible. In the transient case $\mathcal{S}_{\text{NS}}^{-1}$ can be further approximated by the inverse of the stationary Schur complement plus an extra term $-\Delta t L_p^{-1}$ [26], where L_p corresponds to the Poisson problem for p with Neumann boundary conditions. In our numerical examples this extra term makes little difference as we only consider timesteps $\frac{1}{\Delta t} \ll \gamma$, and we therefore neglect it.

Since the augmented Lagrangian term has a large kernel that consists of all solenoidal vector fields, a robust multigrid scheme as described in Section 3.3 must be used to solve the augmented momentum block. For the $\mathbf{H}(\text{div}) \times L^2$ -conforming discretization the *star iteration* [23, section 4] can be used as a robust relaxation method. The subspace decomposition is defined as

$$(3.28) \quad \mathbf{V}_i = \{\mathbf{v} \in \mathbf{V}_h : \text{supp}(\mathbf{v}) \subset K_i\}$$

where K_i is the patch of elements sharing the vertex i in the mesh. Example patches are shown in Figure 3.1. Since we use a structure-preserving discretization, the properties of the de Rham complexes (2.13) and (2.14) imply that (3.28) fulfils the kernel decomposition property (3.25). This property was also used in [6] to construct a

robust smoother for the $\mathbf{H}(\text{div})$ and $\mathbf{H}(\text{curl})$ Riesz maps and in [27] for the Stokes equations. In this case we may employ the standard prolongation operator induced by the finite element discretization, because the uniformly-refined mesh hierarchy we consider is nested.

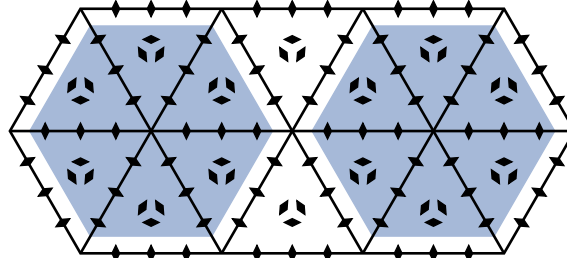


Fig. 3.1: Star patch for \mathbb{BDM}_2 -elements.

The velocity block further includes terms given by the convection-diffusion term $(\mathbf{u} \cdot \nabla)\mathbf{u}$, the linearization of the Lorentz force $S \mathbf{B}^n \times (\mathbf{u} \times \mathbf{B}^n)$ and the stabilization term (2.16). Numerical experiments in [22] and in the next Section 4 show that these terms do not notably degrade the performance of the preconditioner. The kernel of the stabilization $\mathcal{ST}(\mathbf{u}, \mathbf{v})$ consists of all C^1 vector fields. Therefore, the stabilization term slightly degrades the performance of the solver, but the impact is not very significant as the factor $\mu h_{\partial K}^2$ is small.

3.5. Solver for the electromagnetic block. The weak formulation of the electromagnetic block is given by

$$(3.29) \quad \begin{aligned} (\mathbf{E}, \mathbf{F}) - (\mathbf{B}, \mathbf{curl} \mathbf{F}) + \delta (\mathbf{u}^n \times \mathbf{B}, \mathbf{F}) &= 0 & \forall \mathbf{F} \in \mathbf{H}_0(\text{curl}, \Omega), \\ \frac{\eta}{\Delta t} (\mathbf{B}, \mathbf{C}) + (\mathbf{curl} \mathbf{E}, \mathbf{C}) + (\text{div} \mathbf{B}, \text{div} \mathbf{C}) &= (\mathbf{f}, \mathbf{C}) & \forall \mathbf{C} \in \mathbf{H}_0(\text{div}, \Omega). \end{aligned}$$

Eliminating \mathbf{E} , this corresponds to a mixed formulation of

$$(3.30) \quad \begin{aligned} \frac{\eta}{\Delta t} \mathbf{B} + \frac{1}{\text{Re}_m} (\mathbf{curl} \mathbf{curl} \mathbf{B} - \nabla \text{div} \mathbf{B}) + \delta \mathbf{curl}(\mathbf{u}^n \times \mathbf{B}) &= \mathbf{f} \text{ in } \Omega, \\ \mathbf{B} \cdot \mathbf{n} &= 0 \text{ on } \partial\Omega, \\ \frac{1}{\text{Re}_m} \mathbf{curl} \mathbf{B} - \delta \mathbf{u}^n \times \mathbf{B} &= \mathbf{0} \text{ on } \partial\Omega. \end{aligned}$$

For the Picard linearization, this problem simplifies to the mixed formulation for the standard vector Laplace problem [7] with boundary conditions $\mathbf{B} \cdot \mathbf{n} = \mathbf{curl} \mathbf{B} = \mathbf{0}$ on $\partial\Omega$. Chen et al. [15] propose a Schur complement solver and Arnold et al. [7, §10] propose a norm-equivalent block diagonal preconditioner for the mixed formulation. We also found that the star multigrid solver applied monolithically to the electromagnetic block (3.30) results in an efficient solver and employ this solver in our numerical examples. All of the solvers described show Re_m -robust performance.

In contrast, the presence of the additional term $\mathbf{curl}(\mathbf{u}^n \times \mathbf{B})$ in the Newton and MDP iteration, which has a non-trivial kernel, makes the problem almost singular for high Re_m in the stationary case and hence requires a special multigrid method.

Unfortunately the troublesome term $\mathbf{curl}(\mathbf{u}^n \times \mathbf{B})$ is not symmetric and thus does not fit the available analytical framework of Schöberl. Our considerations on this point are therefore necessarily heuristic. Some insight may be gained by employing the vector identity

$$(3.31) \quad \mathbf{curl}(\mathbf{A} \times \mathbf{B}) = (\mathbf{B} \cdot \nabla) \mathbf{A} - (\mathbf{A} \cdot \nabla) \mathbf{B} + \mathbf{A}(\nabla \cdot \mathbf{B}) - \mathbf{B}(\nabla \cdot \mathbf{A})$$

to simplify (3.30) to

$$(3.32) \quad \frac{\eta}{\Delta t} \mathbf{B} - \frac{1}{\text{Re}_m} \Delta \mathbf{B} - (\mathbf{B} \cdot \nabla) \mathbf{u}^n + (\mathbf{u}^n \cdot \nabla) \mathbf{B} - \mathbf{u}^n(\nabla \cdot \mathbf{B}) - \mathbf{B}(\nabla \cdot \mathbf{u}^n).$$

The last term $-\mathbf{B}(\nabla \cdot \mathbf{u}^n)$ vanishes since we exactly enforce $\nabla \cdot \mathbf{u}^n = 0$ in each step. The terms $-(\mathbf{B} \cdot \nabla) \mathbf{u}^n + (\mathbf{u}^n \cdot \nabla) \mathbf{B}$ are reminiscent of the Newton linearization of the advection term $(\mathbf{u} \cdot \nabla) \mathbf{u}$ of the Navier–Stokes equation, for which it has been established that a star multigrid method is effective. Numerical experiments with these approaches applied monolithically do indeed yield a robust solver for the stationary and transient cases in two dimensions, and in the transient case in three dimensions for sufficiently small Δt . In three dimensions the solver breaks down for $\text{Re}_m \approx 700$ for a stationary lid-driven cavity problem.

4. Numerical results. In this section, we present numerical results for the Picard, minimal decoupling Picard and Newton linearizations described in the previous sections. We investigate three test problems: the stationary Hartmann problem, a stationary generator problem, and the stationary and transient versions of a lid-driven cavity problem. The numerical results were measured on a compute cluster that consists of 755GB of RAM and 72 2.3 GHz Intel Xeon cores, of which we used 8 cores at a time for a single calculation.

4.1. Algorithm details. The algorithm is implemented in Firedrake [40] and uses the solver packages PETSc [8] and PCPATCH [21]. The latter includes the implementation of the multigrid relaxation method described in Section 3. It is well-known that the convergence of the nonlinear scheme heavily depends on the initial guess and might fail to converge for high Reynolds numbers with poor initial guesses. To circumvent this problem we perform continuation in the Reynolds numbers and coupling number for the stationary problems. We first apply continuation to one variable while the other variable is fixed. Each solution in the first continuation is then used as the starting point for the continuation in the second variable, to investigate how our solver scales across parameter space.

We use flexible GMRES [42] as the outermost Krylov solver since we apply GMRES in the multigrid relaxation. Moreover, we apply a full block factorization preconditioner [9]

$$(4.1) \quad \mathcal{P} = \begin{pmatrix} \mathcal{I} & -\tilde{\mathcal{M}}^{-1} \mathcal{K} \\ \mathbf{0} & \mathcal{I} \end{pmatrix} \begin{pmatrix} \tilde{\mathcal{M}}^{-1} & \mathbf{0} \\ \mathbf{0} & \tilde{\mathcal{S}}^{-1} \end{pmatrix} \begin{pmatrix} \mathcal{I} & \mathbf{0} \\ -\mathcal{L} \tilde{\mathcal{M}}^{-1} & \mathcal{I} \end{pmatrix}$$

to (2.19), where we denoted (2.19) here as $\begin{pmatrix} \mathcal{M} & \mathcal{K} \\ \mathcal{L} & \mathcal{N} \end{pmatrix}$.

Both the block matrix \mathcal{M} and the outer Schur complement approximation $\mathcal{S}_{\text{MDP}}^{(\mathbf{u}, p)}$ are inverted approximately with two iterations of preconditioned FGMRES (denoted $\tilde{\mathcal{M}}^{-1}$ and $\tilde{\mathcal{S}}^{-1}$ respectively). The former uses the block preconditioner for the hydrodynamic block described in Section 3.4, the latter the monolithic multigrid method

described in Section 3.5. In the numerical results we focus on taking the outer Schur complement that eliminates the hydrodynamic block, except for one case in Section 4.4.2. In both multigrid methods we use six preconditioned GMRES iterations as the smoother on each level and the direct solver MUMPS [3] to solve the problem on the coarsest grid. Since this relaxation is quite expensive, convergence in a very small number of outer iterations is required for efficiency. See Figure 4.1 for a graphical representation of the solver.

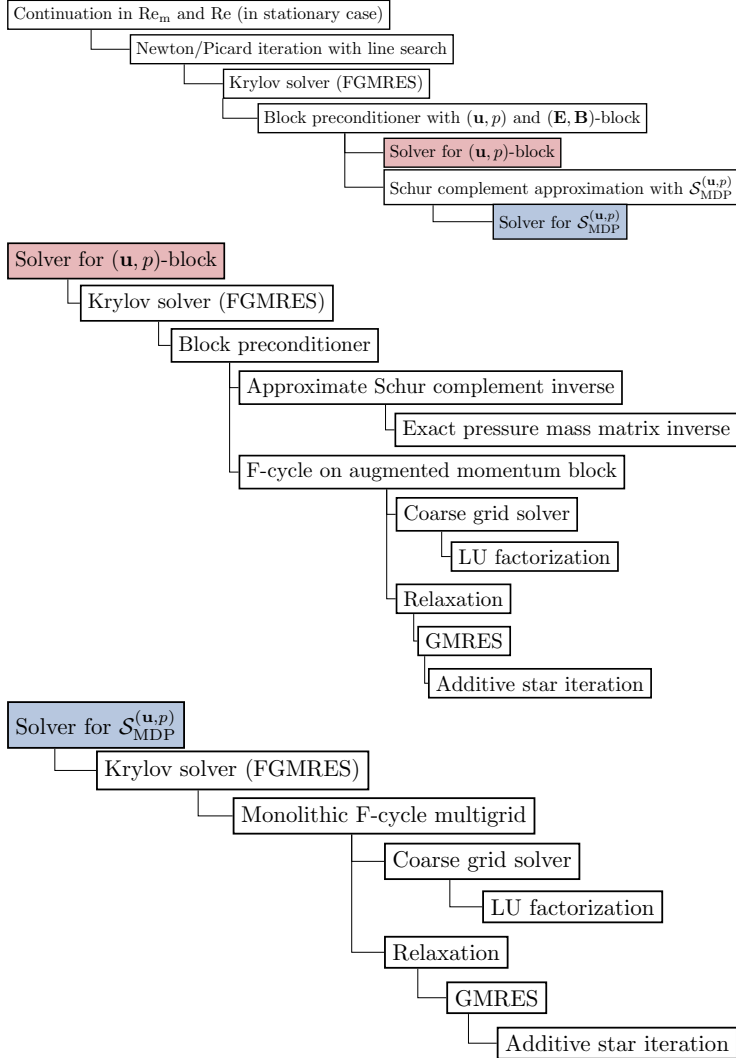


Fig. 4.1: Graphical outline of the solver.

We have chosen relative and absolute tolerances of 10^{-10} and 10^{-6} for the non-linear solver and 10^{-7} and 10^{-7} for the outermost linear solver, measured in the Euclidean norm. We use the $\mathbf{H}(\text{div}) \times L^2$ -conforming elements $\mathbb{BDM}_2 \times \mathbb{DG}_1$ for (\mathbf{u}_h, p_h) . Moreover, we apply $\mathbb{CG}_2 \times \mathbb{RT}_2$ elements for (E_h, \mathbf{B}_h) in 2D and $\mathbb{NED}1_2 \times \mathbb{RT}_2$ elements for $(\mathbf{E}_h, \mathbf{B}_h)$ in 3D. All problems are posed over the domain $\Omega = [-1/2, 1/2]^d$,

unless stated otherwise. For the multigrid hierarchy we use a coarse mesh of 20×20 (resp. $8 \times 8 \times 8$) cells and two (resp. one) level(s) of refinement in 2D (resp. 3D). When we consider a manufactured solution we always subtract $\int_{\Omega} p \, dx$ from the pressure to fix the average of p to be zero.

For time-dependent problems, we apply the second-order, L-stable BDF2 method with a fixed time-step. We compute the first time-step with Crank-Nicolson to provide the second starting value for BDF2. In all the tests, we use a time-step of $\Delta t = 0.01$ and a final time of $T = 0.1$. We did not choose a higher final time T because of computational limitations. However, we confirmed that the reported numbers are representative for higher T by computing the solution for a few parameters until $T = 1$ without noticeable changes in the iteration counts.

4.2. Interpolating boundary data. The theory from the previous sections has been formulated for homogeneous boundary conditions, but the generalisation is straightforward for non-homogeneous boundary conditions. However, there is a subtle technicality in the implementation if one wants to enforce the divergence constraint $\operatorname{div} \mathbf{B}_h = 0$ pointwise. Strong boundary conditions are enforced in a finite element code by interpolating the given boundary data onto the corresponding finite element space. If the interpolation of the boundary values \mathbf{g} were exact, identity (2.15) would imply that $\operatorname{div} \mathbf{B}_h = 0$ holds. However, the degrees of freedom for the interpolation are moments and are usually implemented by a quadrature rule whose quadrature degree is based on the polynomial degree of the finite element space. If \mathbf{g} is a non-polynomial expression, this quadrature rule might not interpolate the boundary condition exactly and therefore one loses the property that $\operatorname{div} \mathbf{g}_h = 0$ on $\partial\Omega$ holds exactly.

To circumvent this problem we use high-order quadrature rules for the evaluation of the degrees of freedom to ensure that the interpolation is exact up to machine precision. In Figure 4.2 we have illustrated the effect of the quadrature degree on the enforcement of the divergence constraint. We have used the method of manufactured solutions for a smooth problem to compute $\|\operatorname{div} \mathbf{B}_h\|_0$ for different quadrature degrees. Moreover, we have plotted the L^2 -norm over $\partial\Omega$ of the interpolation of the divergence-free function \mathbf{B} into the \mathbb{RT}_2 space. One can clearly observe that a quadrature degree of 2 for \mathbb{RT}_2 elements is not sufficient to enforce $\operatorname{div} \mathbf{B}_h = 0$ up to machine precision. A higher quadrature degree preserves the divergence of the boundary data more accurately and leads to the point-wise enforcement of $\operatorname{div} \mathbf{B}_h = 0$.

4.3. Two-dimensional results.

4.3.1. Hartmann flow. First, we consider the Hartmann flow problem that describes the flow of a conducting fluid through a section of a channel to which a transverse magnetic field $\mathbf{B}_0 = (0, 1)^\top$ is applied. This problem was considered in [1, 49]. The analytical solution is given by $\mathbf{u} = (u_1(y), 0)^\top$ and $\mathbf{B} = (B_1(y), 1)^\top$ with

$$\begin{aligned} u_1(y) &= \frac{G\operatorname{Re}}{2\operatorname{Ha} \tanh(\operatorname{Ha}/2)} \left(1 - \frac{\cosh(y\operatorname{Ha})}{\cosh(\operatorname{Ha}/2)} \right), \\ B_1(y) &= \frac{G}{2} \left(\frac{\sinh(y/\operatorname{Ha})}{\sinh(\operatorname{Ha}/2)} - 2y \right), \\ p(x, y) &= -Gx - \frac{B_1^2(y)}{2}. \end{aligned}$$

Here, we used the Hartmann number $\operatorname{Ha} = \sqrt{S\operatorname{Re}\operatorname{Re}_m}$ and $G = \frac{2\operatorname{Ha}\sinh(\operatorname{Ha}/2)}{\operatorname{Re}(\cosh(\operatorname{Ha}/2)-1)}$. The analytical solution for E is computed via (1.3c). Note that for high Ha the

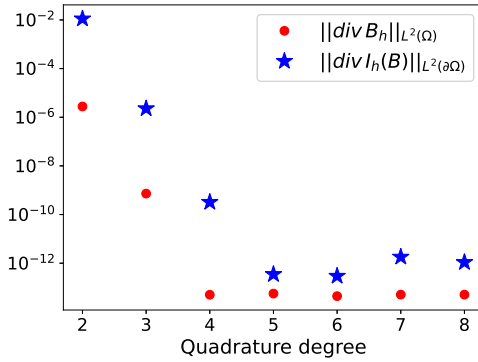


Fig. 4.2: L^2 -norm of the divergence of the solution \mathbf{B}_h and the interpolant of the boundary condition for different quadrature degrees in the evaluation of the degrees of freedom for the Raviart–Thomas space.

computation of, e.g., $\sinh(\text{Ha}/2)$ exceeds the range that double precision floating point numbers can represent. Therefore, we have chosen the following approximation for Hartmann numbers $\text{Ha} \geq 100$ with $G = 2 \frac{\text{Ha}}{\text{Re}}$

$$u_1(y) = \frac{G\text{Re}}{2\text{Ha}} \left(1 + \exp(\text{Ha}(-y - \frac{1}{2})) - \exp(\text{Ha}(y - \frac{1}{2})) \right),$$

$$B_1(y) = \frac{G}{2} \left(\exp(\text{Ha}(-y - \frac{1}{2})) - \exp(\text{Ha}(y - \frac{1}{2})) - 2y \right).$$

The iteration counts for the three different linearization methods are presented in Table 4.1. For all three schemes, we observe fairly constant Krylov iteration counts for Re and S in the range of 1 to 10,000. In terms of the nonlinear convergence, the Picard linearization takes more iterations than the minimal decoupling Picard and Newton linearizations. For higher S in the range up to 100,000 the nonlinear convergence of the Picard iteration deteriorates and finally fails to converge within 25 nonlinear iterations, while the other two schemes remain robust. The Krylov iterations of all three methods remain fairly constant. This is due to the fact that we have good control over the outer Schur complement and that we have robust solvers for both the electromagnetic block and the outer Schur complement.

4.3.2. Stationary lid-driven cavity in two dimensions. Next, we consider a lid-driven cavity problem for a background magnetic field $\mathbf{B}_0 = (0, 1)^\top$ which determines the boundary conditions $\mathbf{B} \cdot \mathbf{n} = \mathbf{B}_0 \cdot \mathbf{n}$ on $\partial\Omega$ and $\mathbf{f} = \mathbf{0}$ [33]. We impose the boundary condition $\mathbf{u} = (1, 0)^\top$ at the boundary $y = 0.5$ and homogeneous boundary conditions elsewhere. The problem models the flow of a conducting fluid driven by the movement of the lid at the top of the cavity. The magnetic field imposed orthogonal to the lid creates a Lorentz force that perturbs the flow of the fluid. For this problem, the iteration counts in Table 4.2 for different S and Re are very similar for the three linearization methods that we have investigated.

As mentioned earlier, our scheme does not include a stabilization for high magnetic Reynolds numbers. However, we have verified that our solutions do not exhibit oscillations in this regime. A plot of the streamlines for different Re and Re_m can be found in Figure 4.3. One can clearly observe the phenomenon that for high magnetic

		Picard			MDP			Newton		
$S \setminus Re$	1	1,000	10,000	1	1,000	10,000	1	1,000	10,000	
1	(4) 5.2	(2) 4.5	(3) 6.3	(3) 5.0	(2) 4.5	(3) 6.3	(3) 5.0	(2) 4.5	(3) 6.3	
10,000	(5) 5.2	(6) 4.7	(5) 3.2	(3) 6.3	(2) 6.5	(2) 5.0	(2) 6.0	(2) 7.0	(2) 5.0	
100,000	(8) 7.4	(19) 4.0	-	(4) 9.8	(4) 12.8	(2) 8.5	(3) 8.7	(3) 8.3	(2) 9.5	

Table 4.1: (Nonlinear iterations) Average outer Krylov iterations per nonlinear step and for the stationary Hartmann problem in 2D.

		Picard			MDP			Newton		
$S \setminus Re$	1	1,000	10,000	1	1,000	10,000	1	1,000	10,000	
1	(4) 5.0	(4) 4.5	(3) 6.7	(2) 6.5	(3) 5.7	(3) 6.7	(2) 6.5	(3) 5.7	(3) 6.7	
10,000	(3) 6.0	(3) 5.7	(2) 8.0	(3) 6.0	(3) 5.7	(2) 8.0	(2) 7.0	(2) 8.0	(2) 8.0	
100,000	(3) 7.7	(3) 8.3	(2) 9.0	(3) 8.0	(3) 8.3	(2) 9.0	(2) 10.0	(2) 11.0	(2) 9.0	

Table 4.2: (Nonlinear iterations) Average outer Krylov iterations per nonlinear step for the stationary lid-driven cavity problem in 2D.

Reynolds numbers the magnetic field lines are advected with the fluid flow. Iteration counts are displayed in Table 4.3.

For the Picard linearization we observe that the nonlinear scheme already fails to converge for a magnetic Reynolds number of 100. The poor nonlinear convergence of the Picard iteration for high Re_m even with continuation was previously observed for other formulations [37, 38].

For the minimal decoupling Picard linearization we observe that the linear solver is also robust with respect to the magnetic Reynolds number, with a slight exception for $Re_m = 10,000$ and $Re = 1$. This indicates that the linear solver for the $(\mathbf{E}_h, \mathbf{B}_h)$ block described in Section 3.5 works very well for high Re_m . However, due to the omission of the matrix \mathcal{G} from the nonlinear scheme one can see an increase in the number of nonlinear iterations.

For the Newton linearization the linear iterations increase slightly since the approximation of the Schur complement $\mathcal{S}_N^{(u,p)}$ by $\mathcal{S}_{MDP}^{(u,p)}$ becomes less accurate for high Reynolds numbers. On the other hand, the number of nonlinear iterations remains fairly constant.

Note that the cost per Krylov iteration is approximately the same for the Newton and minimal decoupling Picard iterations. Hence, a good estimate for the overall cost of the preconditioner is given by the product of the Krylov and nonlinear iterations. We can see that for high Re_m the Newton iteration clearly outperforms the minimal decoupling Picard iteration.

4.3.3. Scott–Vogelius discretization for (\mathbf{u}_h, p_h) . Thus far all presented iteration numbers were computed for the $\mathbf{H}(\text{div}) \times L^2$ discretization for the hydrodynamic variables. For comparison, in this subsection we include results for Scott–Vogelius elements [45], i.e. $(\mathbb{C}\mathbb{G}_k)^d \times \mathbb{D}\mathbb{G}_{k-1}$ elements. A fluid-Reynolds-robust preconditioner for this element pair was recently developed in [22]. While this conforming discretization does not require stabilization terms to weakly enforce continuity, it is only stable on certain types of meshes. For this reason, the mesh hierarchy is barycentrically refined, and the specialized multigrid method of [22] exploits this structure. This barycentric

		Picard			MDP			Newton		
Re _m \Re		1	1,000	10,000	1	1,000	10,000	1	1,000	10,000
1	(4)	5.0	(4)	4.5	(3)	6.7	(2)	6.5	(3)	5.7
1,000	-	-	-	-	(2)	6.5	(12)	5.2	(9)	7.1
10,000	-	-	-	-	(2)	22.5	(14)	6.1	(16)	6.8

Table 4.3: Iteration counts for the stationary lid-driven cavity problem in 2D with $\mathbf{H}(\text{div}) \times L^2$ -discretization for different Re_m and Re .

		Picard			MDP			Newton		
Re _m \Re		1	1,000	10,000	1	1,000	10,000	1	1,000	10,000
1	(3)	2.3	(3)	2.7	(2)	5.0	(2)	3.0	(3)	2.7
1,000	-	-	-	-	(6)	2.5	(8)	2.2	(4)	4.8
10,000	-	-	-	-	(9)	4.1	(9)	3.1	(6)	4.7

Table 4.4: Iteration counts for the stationary lid-driven cavity problem in 2D with Scott–Vogelius elements for different Re_m and Re .

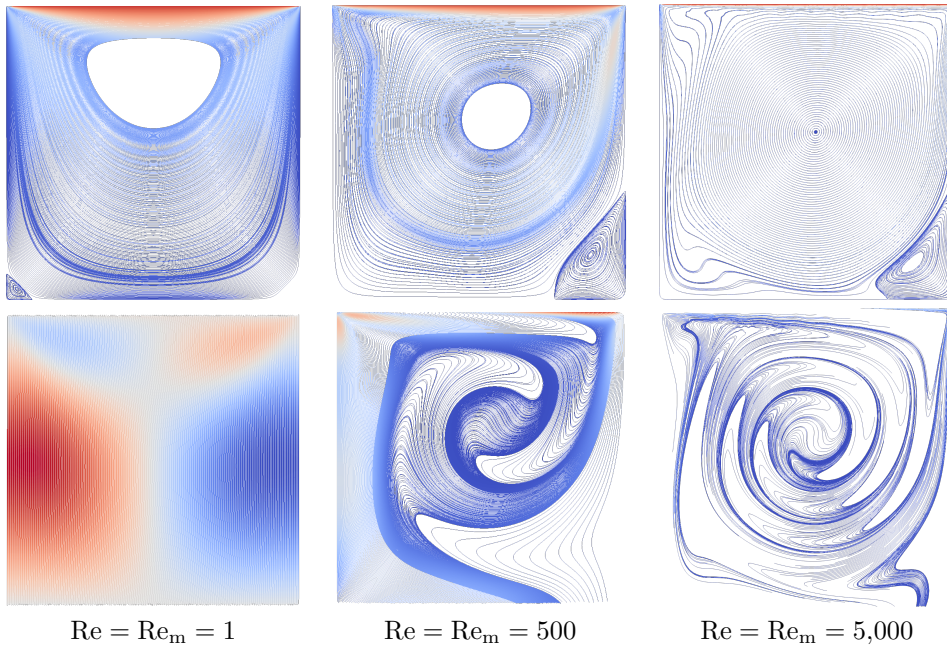


Fig. 4.3: Streamlines for the two-dimensional stationary lid-driven cavity problem for \mathbf{u} (upper row) and \mathbf{B} (lower row).

refinement ensures stability for polynomial order $k = d$ [54].

The results are shown in Table 4.4. We observe that the Krylov iteration counts are in general lower for the Scott–Vogelius element, making this an attractive alternative for those wishing to employ conforming schemes. However, one must keep in mind that the work per Krylov iteration is substantially higher for this element, due

to the use of larger patches in the so-called macrostar relaxation method.

To summarize the two-dimensional stationary results, all schemes considered provide Re-robust solvers and also perform very well for large coupling numbers S . The Picard iteration is unsuitable for high magnetic Reynolds number because the nonlinear iteration fails to converge. Both the minimal decoupling Picard and Newton scheme perform well for high Re_m with the tradeoff that the minimal decoupling Picard iteration provides a robust linear solver while the Newton scheme shows better nonlinear convergence.

4.3.4. Time-dependent lid-driven cavity problem in two dimensions.

We next consider the time-dependent lid-driven cavity problem. We choose the same boundary conditions and right-hand side as in the stationary case. The numerical results for different S and Re are shown in Table 4.5. As in the stationary case, the Krylov iteration counts remain almost constant for the three linearizations. The nonlinear iteration counts of the Picard and minimal decoupling Picard iteration increase for high S , while they remain constant for the Newton scheme.

For different Re and Re_m we see in Table 4.5 a fully robust scheme for the MDP and Newton iterations. As in the stationary case, we observe that the Picard scheme has nonlinear convergence problems for high Re_m .

For completeness, we also study the case of high Re_m and S at the same time in Table 4.5, which we expect to be the most challenging case. Here, we see that the nonlinear MDP iteration fails to converge for $S = 10,000$ and $Re_m = 1,000$ and higher. Again the Newton scheme shows the best convergence. The slight increase of the Krylov iterations is due to inaccurate outer Schur complement approximation. However, the solvers perform very well, considering the difficulty of the problem.

		Picard			MDP			Newton		
$S \setminus Re$	1	10,000	100,000	1	10,000	100,000	1	10,000	100,000	
1	(2.0) 3.7	(2.2) 1.9	(2.3) 1.7	(1.7) 4.5	(2.2) 1.9	(2.3) 1.6	(1.6) 4.4	(2.2) 1.9	(2.3) 1.7	
1,000	(3.0) 5.8	(2.7) 2.6	(2.9) 2.2	(3.5) 7.4	(4.2) 2.6	(4.2) 2.0	(2.1) 6.9	(2.3) 2.9	(2.4) 2.4	
10,000	(3.3) 7.5	(5.2) 3.0	(5.6) 2.5	(5.6) 10.2	(5.8) 5.3	(5.7) 4.4	(2.2) 9.2	(2.2) 5.3	(2.2) 4.5	

		Picard			MDP			Newton		
$Re_m \setminus Re$	1	10,000	100,000	1	10,000	100,000	1	10,000	100,000	
1	(2.0) 3.7	(2.2) 1.9	(2.3) 1.7	(1.7) 4.5	(2.2) 1.9	(2.3) 1.6	(1.6) 4.4	(2.2) 1.9	(2.3) 1.7	
10,000	-	(7.0) 1.3	(3.8) 1.4	(2.2) 4.3	(2.5) 1.8	(2.4) 1.6	(2.1) 4.4	(2.1) 1.9	(2.3) 1.7	
100,000	-	-	(5.1) 1.5	(2.3) 4.9	(3.0) 1.7	(2.5) 1.6	(2.1) 5.1	(2.2) 2.0	(2.4) 1.7	

		Picard			MDP			Newton		
$Re_m \setminus S$	1	1,000	10,000	1	1,000	10,000	1	1,000	10,000	
1	(2.0) 3.7	(3.0) 5.8	(3.3) 7.5	(1.7) 4.5	(3.5) 7.4	(5.6) 10.2	(1.6) 4.4	(2.1) 6.9	(2.2) 9.2	
1,000	-	-	-	(2.2) 3.9	(4.7) 6.7	-	(2.1) 3.9	(2.2) 8.2	(2.7) 14.4	
10,000	-	-	-	(2.2) 4.3	(5.2) 6.7	-	(2.1) 4.4	(2.5) 8.1	(3.2) 14.5	

Table 4.5: Iteration counts for the transient lid-driven cavity problem in 2D.

4.4. Three-dimensional results. In three dimensions, we observe in general that the stationary problems are harder to solve for high parameters than in two dimensions. We believe that the following three points are mainly responsible for this behavior. First of all, the discretization of the electric field changes from a

scalar-valued \mathbb{CG} -function to a vector-valued NED1 -function with tangential boundary conditions. Moreover, the kernel of the term $\mathbf{curl}(\mathbf{u}^n \times \mathbf{B})$ is larger in three dimensions which degrades the performance of the monolithic solver for the $(\mathbf{E}_h, \mathbf{B}_h)$ block for high Re_m . Furthermore, the grids we consider are much coarser than in two dimensions because of computational costs.

4.4.1. MHD generator. We consider a stationary generator problem which models the flow in a duct that generates an electric current [1, 39, 48]. Here, we consider the domain $\Omega = [0, 5] \times [0, 1] \times [0, 1]$. For \mathbf{B} we impose on $z = 0$ and $z = 1$ the normal boundary conditions $\mathbf{B} \cdot \mathbf{n} = (0, 0, b_z(x))^\top \cdot \mathbf{n}$ with

$$(4.2) \quad b_z(x) = \frac{B_0}{2} \left(\tanh\left(\frac{x - x_{\text{on}}}{\delta}\right) - \tanh\left(\frac{x - x_{\text{off}}}{\delta}\right) \right)$$

and $B_0 = 1, \delta = 0.1, x_{\text{on}} = 2.0$ and $x_{\text{off}} = 2.5$. Note that these normal boundary conditions lead to the same solution as the tangential boundary conditions considered in [1, 39, 48]. For \mathbf{u} we impose inflow Dirichlet boundary conditions $(1, 0, 0)^\top$ on $x = 0$ and natural outflow boundary conditions on $x = 5$. On the other four walls, we set $\mathbf{u} = (0, 0, 0)^\top$. Finally, we choose homogeneous boundary conditions for \mathbf{E} .

In Table 4.6 we report iteration counts for S and Re . For this problem, we observe good convergence for all three methods if either $S = 1$ or $\text{Re} = 1$. Surprisingly, if both parameters are chosen relatively high, nonlinear convergence of the minimal decoupling Picard iteration is not observed within 25 iterations. This is a marked difference in comparison to the results in 2D. For the Picard and Newton iteration we observe an increase in the Krylov iteration counts. We confirmed numerically that the main source of the increase in the Krylov iteration counts is the Schur complement approximation by applying a direct solver to it and the Navier–Stokes block.

4.4.2. Stationary lid-driven cavity problem in three dimensions. We adapt the two-dimensional lid-driven cavity problem to three dimensions by considering boundary conditions $\mathbf{u} = (1, 0, 0)^\top$ on the boundary $y = 1$ and $\mathbf{u} = (0, 0, 0)^\top$ on the other faces. The background magnetic field $\mathbf{B}_0 = (0, 1, 0)^\top$ determines the boundary conditions for \mathbf{B} . For the three-dimensional problem, the results in Table 4.7 are similar to the MHD generator problem. The MDP iteration struggles with nonlinear convergence. For this test problem, the case of $\text{Re} = 10,000$ and $S = 1$ seems to be the most challenging, with better convergence for high S in comparison to the generator problem.

In Table 4.8 we report a comparison to taking the outer Schur complement that eliminates the $(\mathbf{E}_h, \mathbf{B}_h)$ block. As mentioned in Section 3, we clearly see an increase in the Krylov iteration counts for high S for the Picard and Newton linearizations. We observed similar behavior for unreported experiments on transient and two-dimensional problems.

We do not include a full table for high Re_m , as in this case the monolithic multigrid solver cannot deal with the term $\mathbf{curl}(\mathbf{u}^n \times \mathbf{B}^n)$ that occurs in the Newton and minimal decoupling Picard linearizations. As in two dimensions, this term is crucial for the convergence of the nonlinear iteration. For Newton, the iteration counts increase very slightly from $\text{Re} = \text{Re}_m = 1$ by 8.0 Krylov iterations per nonlinear step to 10.0 iterations for $\text{Re}_m = 500$ and $\text{Re} = 1$ and fails to converge for higher Re_m . We want to emphasize that in this case the failure of convergence is indeed caused by the inner multigrid method and not by an inaccurate outer Schur complement approximation. To the best of our knowledge, preconditioning methods that robustly treat the vector

		Picard			MDP			Newton		
$S \setminus Re$	1	100	1,000	1	100	1,000	1	100	1,000	
1	(6) 7.0	(7) 5.6	(7) 8.3	(3) 8.3	(4) 8.5	(6) 11.0	(3) 8.3	(4) 7.8	(5) 10.6	
100	(8) 5.5	(9) 6.8	(8) 10.5	(5) 8.8	-	-	(2) 7.5	(4) 8.0	(5) 12.6	
1,000	(10) 6.2	(9) 18.2	(8) 27.6	(18) 10.1	-	-	(3) 7.0	(4) 16.2	(5) 26.2	

Table 4.6: Iteration counts for the stationary generator problem in 3D.

		Picard			MDP			Newton		
$S \setminus Re$	1	1,000	10,000	1	1,000	10,000	1	1,000	10,000	
1	(4) 7.5	(4) 7.2	(4) 21.5	(3) 8.3	(20) 4.8	-	(3) 8.0	(4) 7.2	(4) 21.5	
1,000	(4) 6.8	(3) 9.7	(2) 6.0	(20) 8.0	-	-	(2) 9.0	(3) 8.7	(2) 6.0	
10,000	(5) 8.6	(3) 11.7	(2) 7.0	(18) 9.3	-	-	(4) 8.5	(2) 16.0	(2) 7.5	

Table 4.7: Iteration counts for the stationary lid-driven cavity problem in 3D.

		Picard			MDP			Newton		
$S \setminus Re$	1	1,000	10,000	1	1,000	10,000	1	1,000	10,000	
1	(4) 7.5	(4) 14.2	(4) 36.8	(3) 8.3	(20) 4.8	-	(3) 8.0	(4) 14.5	(4) 37.0	
1,000	(4) 10.5	(3) 38.0	(2) 51.0	(20) 8.2	-	-	(2) 14.0	(3) 34.7	(2) 51.0	
10,000	(5) 17.8	(2) 71.5	(2) 57.5	(18) 9.3	-	-	(4) 18.0	(2) 72.0	(2) 57.5	

Table 4.8: Iteration counts for the stationary lid-driven cavity problem in 3D for taking the outer Schur complement that eliminates the $(\mathbf{E}_h, \mathbf{B}_h)$ block. Compare with Table 4.7.

Laplace operator with an additional $\mathbf{curl}(\mathbf{u}^n \times \mathbf{B})$ term in three dimensions are not known, and we intend to investigate this problem further in future work.

4.4.3. Time-dependent lid-driven cavity problem in three dimensions.

Finally, we consider the time-dependent version of the three-dimensional lid-driven cavity problem, which was also investigated in detail in [33]. The numerical results in Table 4.9 show two main differences to the stationary case. First of all, we observe good nonlinear convergence of the minimal decoupling Picard iteration as long as Re_m and S are not chosen to both be very high. Moreover, we observe robust converge of the monolithic multigrid solver for the $(\mathbf{E}_h, \mathbf{B}_h)$ block for high Re_m . As mentioned before in Section 3.5, this can be explained by the fact that the problem does not become nearly singular for high Re_m due to the extra mass matrix. Therefore, the fact that the kernel of $\mathbf{curl}(\mathbf{u}^n \times \mathbf{B})$ is not fully captured by the multigrid method has less influence.

5. Conclusion and outlook. We have presented scalable block preconditioners for an augmented Lagrangian formulation of the incompressible MHD equations that exhibit parameter-robust iteration counts in most cases. We described how to control the outer Schur complement of three linearization types and introduced a special monolithic multigrid method to solve the electromagnetic block. This method is fully Re_m -robust in two dimensions; in three dimensions, it is able to efficiently compute results for higher parameters than was previously possible. Furthermore, our solvers allow the use of fully implicit methods for time-dependent problems. We aim to

		Picard			MDP			Newton		
$S \setminus Re$	1	10,000	100,000	1	10,000	100,000	1	10,000	100,000	
1,000	(2.1) 6.4	(2.4) 1.8	(2.4) 1.6	(2.2) 6.3	(2.4) 1.7	(2.4) 1.6	(2.0) 6.2	(2.4) 1.8	(2.4) 1.6	
	(3.1) 8.2	(3.6) 2.3	-	(5.2) 10.1	(6.5) 2.0	(6.6) 1.6	(2.1) 10.4	(2.4) 3.0	(2.4) 3.2	
	(3.5) 13.4	-	-	(8.0) 12.6	(9.1) 3.7	(9.6) 3.6	(2.3) 17.0	(2.4) 9.6	(2.5) 9.4	

		Picard			MDP			Newton		
$Re_m \setminus Re$	1	10,000	100,000	1	10,000	100,000	1	10,000	100,000	
10,000	(2.1) 6.4	(2.4) 1.8	(2.4) 1.6	(2.2) 6.3	(2.4) 1.7	(2.4) 1.6	(2.0) 6.2	(2.4) 1.8	(2.4) 1.6	
	(9.7) 2.9	(3.4) 1.5	(2.4) 1.7	(2.3) 6.5	(2.9) 1.6	(2.5) 1.6	(2.1) 6.5	(2.4) 1.8	(2.4) 1.7	
	(10.0) 2.9	(3.4) 1.5	(2.4) 1.7	(2.3) 6.5	(2.9) 1.6	(2.5) 1.6	(2.1) 6.7	(2.4) 1.8	(2.4) 1.7	

		Picard			MDP			Newton		
$Re_m \setminus S$	1	1,000	10,000	1	1,000	10,000	1	1,000	10,000	
1,000	(2.1) 6.4	(3.1) 8.2	(3.5) 13.4	(2.2) 6.3	(5.2) 10.1	(8.0) 12.6	(2.0) 6.2	(2.1) 10.4	(2.3) 17.0	
	(7.5) 3.0	(13.9) 4.6	-	(2.3) 6.3	(7.6) 8.9	-	(2.1) 6.4	(2.8) 8.3	(3.2) 17.4	
	(9.7) 2.9	(16.0) 4.8	-	(2.3) 6.5	(8.8) 9.3	-	(2.1) 6.5	(3.0) 9.2	(3.2) 20.3	

Table 4.9: Iteration counts for the transient lid-driven cavity problem in 3D.

include stabilization techniques for high magnetic Reynolds numbers in future work and further investigate how to develop a robust multigrid method for the problem including the term $\mathbf{curl}(\mathbf{u}^n \times \mathbf{B})$. This would enable a more robust solver for the most difficult case of stationary problems in three dimensions at high magnetic Reynolds numbers.

Acknowledgement. The authors would like to thank Kaibo Hu for many useful suggestions and discussions.

Code availability. The code that was used to generate the numerical results and all major Firedrake components have been archived on [53].

REFERENCES

- [1] J. H. ADLER, T. R. BENSON, E. C. CYR, P. E. FARRELL, S. P. MACLACHLAN, AND R. S. TUMINARO, *Monolithic multigrid for magnetohydrodynamics*, SIAM Journal on Scientific Computing, (2021), <https://arxiv.org/abs/2006.15700>. To appear.
- [2] J. H. ADLER, T. R. BENSON, E. C. CYR, S. P. MACLACHLAN, AND R. S. TUMINARO, *Monolithic multigrid methods for two-dimensional resistive magnetohydrodynamics*, SIAM Journal on Scientific Computing, 38 (2016), pp. B1–B24, <https://doi.org/10.1137/151006135>.
- [3] P. R. AMESTOY, I. S. DUFF, J. KOSTER, AND J.-Y. L'EXCELLENT, *A fully asynchronous multi-frontal solver using distributed dynamic scheduling*, SIAM Journal on Matrix Analysis and Applications, 23 (2001), pp. 15–41, <https://doi.org/10.1137/S0895479899358194>.
- [4] F. ARMERO AND J. SIMO, *Long-term dissipativity of time-stepping algorithms for an abstract evolution equation with applications to the incompressible MHD and Navier–Stokes equations*, Computer Methods in Applied Mechanics and Engineering, 131 (1996), pp. 41–90, [https://doi.org/10.1016/0045-7825\(95\)00931-0](https://doi.org/10.1016/0045-7825(95)00931-0).
- [5] D. N. ARNOLD, *Finite Element Exterior Calculus*, Society for Industrial and Applied Mathematics, Dec. 2018, <https://doi.org/10.1137/1.9781611975543>.
- [6] D. N. ARNOLD, R. S. FALK, AND R. WINTHER, *Multigrid in $H(\text{div})$ and $H(\text{curl})$* , Numerische Mathematik, 85 (2000), pp. 197–217, <https://doi.org/10.1007/pl00005386>.
- [7] D. N. ARNOLD, R. S. FALK, AND R. WINTHER, *Finite element exterior calculus, homological techniques, and applications*, Acta Numerica, 15 (2006), pp. 1–155, <https://doi.org/10.1017/S0962492906210018>.
- [8] S. BALAY, S. ABHYANKAR, M. F. ADAMS, J. BROWN, P. BRUNE, K. BUSCHELMAN, L. DALCIN,

V. EIJKHOUT, W. D. GROPP, D. KARPEYEV, D. KAUSHIK, M. G. KNEPLEY, D. A. MAY, L. C. MCINNES, R. T. MILLS, T. MUNSON, K. RUPP, P. SANAN, B. F. SMITH, S. ZAMPINI, H. ZHANG, AND H. ZHANG, *PETSc users manual*, Tech. Report ANL-95/11 - Revision 3.15, Argonne National Laboratory, 2021.

[9] M. BENZI, G. H. GOLUB, AND J. LIESEN, *Numerical solution of saddle point problems*, Acta Numerica, 14 (2005), pp. 1–137, <https://doi.org/10.1017/S0962492904000212>.

[10] D. BOFFI, F. BREZZI, AND M. FORTIN, *Mixed Finite Element Methods and Applications*, Springer Berlin Heidelberg, 2013, <https://doi.org/10.1007/978-3-642-36519-5>.

[11] J. BRACKBILL AND D. BARNES, *The effect of nonzero $\nabla \cdot \mathbf{B}$ on the numerical solution of the magnetohydrodynamic equations*, Journal of Computational Physics, 35 (1980), pp. 426–430, [https://doi.org/10.1016/0021-9991\(80\)90079-0](https://doi.org/10.1016/0021-9991(80)90079-0).

[12] F. BREZZI, J. DOUGLAS, AND L. D. MARINI, *Two families of mixed finite elements for second order elliptic problems*, Numerische Mathematik, 47 (1985), pp. 217–235, <https://doi.org/10.1007/bf01389710>.

[13] E. BURMAN AND P. HANSBO, *Edge stabilization for the generalized Stokes problem: a continuous interior penalty method*, Computer Methods in Applied Mechanics and Engineering, 195 (2006), pp. 2393–2410, <https://doi.org/10.1016/j.cma.2005.05.009>.

[14] L. CHACÓN, *Scalable parallel implicit solvers for 3D magnetohydrodynamics*, Journal of Physics: Conference Series, 125 (2008), p. 012041, <https://doi.org/10.1088/1742-6596/125/1/012041>.

[15] L. CHEN, Y. WU, L. ZHONG, AND J. ZHOU, *MultiGrid preconditioners for mixed finite element methods of the vector Laplacian*, Journal of Scientific Computing, 77 (2018), pp. 101–128, <https://doi.org/10.1007/s10915-018-0697-7>.

[16] E. C. CYR, J. N. SHADID, R. S. TUMINARO, R. P. PAWLOWSKI, AND L. CHACÓN, *A new approximate block factorization preconditioner for two-dimensional incompressible (reduced) resistive MHD*, SIAM Journal on Scientific Computing, 35 (2013), pp. B701–B730, <https://doi.org/10.1137/12088879x>.

[17] W. DAI AND P. R. WOODWARD, *On the divergence-free condition and conservation laws in numerical simulations for supersonic magnetohydrodynamical flows*, The Astrophysical Journal, 494 (1998), pp. 317–335, <https://doi.org/10.1086/305176>.

[18] C. DAVIES, M. POZZO, D. GUBBINS, AND D. ALFE, *Constraints from material properties on the dynamics and evolution of earth's core*, Nature Geoscience, 8 (2015), pp. 678–685, <https://doi.org/10.1038/ngeo2492>.

[19] J. DOUGLAS AND T. DUPONT, *Interior penalty procedures for elliptic and parabolic Galerkin methods*, in Computing Methods in Applied Sciences, vol. 58, Springer Berlin Heidelberg, 1976, pp. 207–216, <https://doi.org/10.1007/BFb0120591>.

[20] H. ELMAN, D. SILVESTER, AND A. WATHEN, *Finite Elements and Fast Iterative Solvers*, Oxford University Press, 2014, <https://doi.org/10.1093/acprof:oso/9780199678792.001.0001>.

[21] P. E. FARRELL, M. G. KNEPLEY, L. MITCHELL, AND F. WECHSUNG, *PCPATCH: software for the topological construction of multigrid relaxation methods*, ACM Transactions on Mathematical Software, (2021), <https://arxiv.org/abs/1912.08516>. To appear.

[22] P. E. FARRELL, L. MITCHELL, L. R. SCOTT, AND F. WECHSUNG, *A Reynolds-robust preconditioner for the Scott–Vogelius discretization of the stationary incompressible Navier–Stokes equations*, The SMAI Journal of Computational Mathematics, 7 (2021), pp. 75–96, <https://doi.org/10.5802/smai-jcm.72>, <https://arxiv.org/abs/2004.09398>.

[23] P. E. FARRELL, L. MITCHELL, AND F. WECHSUNG, *An augmented Lagrangian preconditioner for the 3D stationary incompressible Navier–Stokes equations at high Reynolds number*, SIAM Journal on Scientific Computing, 41 (2019), pp. A3073–A3096, <https://doi.org/10.1137/18m1219370>.

[24] N. R. GAUGER, A. LINKE, AND P. W. SCHROEDER, *On high-order pressure-robust space discretisations, their advantages for incompressible high Reynolds number generalised Beltrami flows and beyond*, The SMAI Journal of Computational Mathematics, 5 (2019), pp. 89–129, <https://doi.org/10.5802/smai-jcm.44>.

[25] J.-F. GERBEAU, C. L. BRIS, AND T. LELIÈVRE, *Mathematical Methods for the Magnetohydrodynamics of Liquid Metals*, Oxford University Press, 2006, <https://doi.org/10.1093/acprof:oso/9780198566656.001.0001>.

[26] T. HEISTER AND G. RAPIN, *Efficient augmented Lagrangian-type preconditioning for the Oseen problem using grad-div stabilization*, Internat. J. Numer. Methods Fluids, 71 (2013), pp. 118–134, <https://doi.org/10.1002/fld.3654>.

[27] Q. HONG, J. KRAUS, J. XU, AND L. ZIKATANOV, *A robust multigrid method for discontinuous Galerkin discretizations of Stokes and linear elasticity equations*, Numerische Mathematik, 132 (2015), pp. 23–49, <https://doi.org/10.1007/s00211-015-0712-y>.

- [28] K. HU, Y. MA, AND J. XU, *Stable finite element methods preserving $\nabla \cdot B = 0$ exactly for MHD models*, Numerische Mathematik, 135 (2016), pp. 371–396, <https://doi.org/10.1007/s00211-016-0803-4>.
- [29] K. HU, W. QIU, AND K. SHI, *Convergence of a B-E based finite element method for MHD models on Lipschitz domains*, Journal of Computational and Applied Mathematics, 368 (2020), p. 112477, <https://doi.org/10.1016/j.cam.2019.112477>.
- [30] K. HU AND J. XU, *Structure-preserving finite element methods for stationary MHD models*, Mathematics of Computation, 88 (2018), pp. 553–581, <https://doi.org/10.1090/mcom/3341>.
- [31] V. JOHN, A. LINKE, C. MERDON, M. NEILAN, AND L. G. REBOLZ, *On the divergence constraint in mixed finite element methods for incompressible flows*, SIAM Review, 59 (2017), pp. 492–544, <https://doi.org/10.1137/15m1047696>.
- [32] L. LI AND W. ZHENG, *A robust solver for the finite element approximation of stationary incompressible MHD equations in 3D*, Journal of Computational Physics, 351 (2017), pp. 254–270, <https://doi.org/10.1016/j.jcp.2017.09.025>.
- [33] Y. MA, K. HU, X. HU, AND J. XU, *Robust preconditioners for incompressible MHD models*, Journal of Computational Physics, 316 (2016), pp. 721–746, <https://doi.org/10.1016/j.jcp.2016.04.019>.
- [34] S. MOLOKOV, R. MOREAU, AND K. MOFFATT, *Magnetohydrodynamics*, Springer Netherlands, 2007, <https://doi.org/10.1007/978-1-4020-4833-3>.
- [35] J.-C. NÉDÉLEC, *Mixed finite elements in \mathbb{R}^3* , Numerische Mathematik, 35 (1980), pp. 315–341, <https://doi.org/10.1007/BF01396415>.
- [36] J.-C. NÉDÉLEC, *A new family of mixed finite elements in \mathbb{R}^3* , Numerische Mathematik, 50 (1986), pp. 57–81, <https://doi.org/10.1007/bf01389668>.
- [37] E. G. PHILLIPS, *Fast solvers and uncertainty quantification for models of magnetohydrodynamics*, PhD thesis, University of Maryland, 2014.
- [38] E. G. PHILLIPS, H. C. ELMAN, E. C. CYR, J. N. SHADID, AND R. P. PAWLOWSKI, *A block preconditioner for an exact penalty formulation for stationary MHD*, SIAM Journal on Scientific Computing, 36 (2014), pp. B930–B951, <https://doi.org/10.1137/140955082>.
- [39] E. G. PHILLIPS, J. N. SHADID, E. C. CYR, H. C. ELMAN, AND R. P. PAWLOWSKI, *Block preconditioners for stable mixed nodal and edge finite element representations of incompressible resistive MHD*, SIAM Journal on Scientific Computing, 38 (2016), pp. B1009–B1031, <https://doi.org/10.1137/16M1074084>.
- [40] F. RATHGEBER, D. A. HAM, L. MITCHELL, M. LANGE, F. LUPORINI, A. T. T. MCRAE, G.-T. BERCEA, G. R. MARKALL, AND P. H. J. KELLY, *Firedrake: automating the finite element method by composing abstractions*, ACM Transactions on Mathematical Software, 43 (2016), pp. 1–27, <https://doi.org/10.1145/2998441>.
- [41] P. A. RAVIART AND J. M. THOMAS, *A mixed finite element method for second order elliptic problems*, in Lecture Notes in Mathematics, Springer Berlin Heidelberg, 1977, pp. 292–315, <https://doi.org/10.1007/bfb0064470>.
- [42] Y. SAAD, *A flexible inner-outer preconditioned GMRES algorithm*, SIAM Journal on Scientific Computing, 14 (1993), pp. 461–469, <https://doi.org/10.1137/0914028>.
- [43] J. SCHÖBERL, *Robust Multigrid Methods for Parameter Dependent Problems*, PhD thesis, Johannes Kepler Universität Linz, Linz, Austria, 1999.
- [44] D. SCHÖTZAU, *Mixed finite element methods for stationary incompressible magnetohydrodynamics*, Numerische Mathematik, 96 (2004), pp. 771–800, <https://doi.org/10.1007/s00211-003-0487-4>.
- [45] L. R. SCOTT AND M. VOGELIUS, *Conforming finite element methods for incompressible and nearly incompressible continua*, in Large Scale Computations in Fluid Mechanics, vol. 22 (Part 2), AMS, 1985, pp. 221–244.
- [46] J. SHADID, R. PAWLOWSKI, J. BANKS, L. CHACÓN, P. LIN, AND R. TUMINARO, *Towards a scalable fully-implicit fully-coupled resistive MHD formulation with stabilized FE methods*, Journal of Computational Physics, 229 (2010), pp. 7649–7671, <https://doi.org/10.1016/j.jcp.2010.06.018>.
- [47] J. SHADID, R. PAWLOWSKI, E. CYR, R. TUMINARO, L. CHACÓN, AND P. WEBER, *Scalable implicit incompressible resistive MHD with stabilized FE and fully-coupled Newton–Krylov–AMG*, Computer Methods in Applied Mechanics and Engineering, 304 (2016), pp. 1–25, <https://doi.org/10.1016/j.cma.2016.01.019>.
- [48] M. WATHEN AND C. GREIF, *A scalable approximate inverse block preconditioner for an incompressible magnetohydrodynamics model problem*, SIAM Journal on Scientific Computing, 42 (2020), pp. B57–B79, <https://doi.org/10.1137/19m1255409>.
- [49] M. WATHEN, C. GREIF, AND D. SCHÖTZAU, *Preconditioners for mixed finite element discretiza-*

tions of incompressible MHD equations, SIAM Journal on Scientific Computing, 39 (2017), pp. A2993–A3013, <https://doi.org/10.1137/16m1098991>.

[50] S. WU AND J. XU, *Simplex-averaged finite element methods for $H(\text{grad})$, $H(\text{curl})$, and $H(\text{div})$ convection-diffusion problems*, SIAM Journal on Numerical Analysis, 58 (2020), pp. 884–906, <https://doi.org/10.1137/18m1227196>.

[51] S. WU AND L. T. ZIKATANOV, *On the unisolvence for the quasi-polynomial spaces of differential forms*, 2020, <https://arxiv.org/abs/2003.14278>.

[52] J. XU, *Iterative methods by space decomposition and subspace correction*, SIAM Review, 34 (1992), pp. 581–613, <https://doi.org/10.1137/1034116>.

[53] *Software used in ‘An augmented Lagrangian preconditioner for the magnetohydrodynamics equations at high Reynolds and coupling numbers’*, April 2021, <https://doi.org/10.5281/zenodo.4723637>.

[54] S. ZHANG, *A new family of stable mixed finite elements for the 3D Stokes equations*, Mathematics of Computation, 74 (2005), pp. 543–555, <https://doi.org/10.1090/s0025-5718-04-01711-9>.